ELSEVIER

Marine Geology 230 (2006) 249–273

MARINE GEOLOGY
INTERNATIONAL JOURNAL OF MARINE GEOLOGY, GEOCHEMISTRY AND GEOPHYSICS

www.elsevier.com/locate/margeo

The structural evolution of the Messinian evaporites in the Levantine Basin

G.L. Netzeband *, C.P. Hübscher [1], D. Gajewski [2]

Institut für Geophysik, Universität Hamburg, Bundesstraße 55, 20146 Hamburg, Germany

Received 23 December 2005; received in revised form 21 April 2006; accepted 31 May 2006

Abstract

The Levantine Basin in the South-eastern Mediterranean Sea is a world class site for studying the initial stages of salt tectonics driven by differential sediment load, because the Messinian evaporites are comparatively young, the sediment load varies along the basin margin, they are hardly tectonically overprinted, and the geometry of the basin and the overburden is well-defined. In this study we analyse depositional phases of the evaporites and their structural evolution by means of high-resolution multi-channel seismic data. The basinal evaporites have a maximum thickness of about 2 km, precipitated during the Messinian Salinity Crisis, 5.3–5.9 Ma ago. The evaporite body is characterized by 5 transparent layers sequenced by four internal reflections. We suggest that each of the internal reflection bands indicate a change of evaporite facies, possibly interbedded clastic sediments, which were deposited during temporal sea level rises. All of these internal reflections are differently folded and distorted, proving that the deformation was syn-depositional. Thrust angles up to 14° are observed. Backstripping of the Pliocene–Quaternary reveals that salt tectonic is mainly driven by the sediment load of the Nile Cone. The direction of lateral salt displacement is mainly SSW–NNE and parallel to the bathymetric trend. Apparent rollback anticlines off Israel result rather from differential subsidence than from lateral salt displacement. In the south-eastern basin margin the deposition of the Isreali Slump Complex (ISC) is coeval with the onset of salt tectonic faulting, suggesting a causal link between slumping processes and salt tectonics.

The superposition of 'thin-skinned' tectonics and 'thick-skinned' tectonics becomes apparent in several locations: The fold belt off the Israeli Mediterranean slope mainly results from active strike-slip tectonics, which becomes evident in faults which reach from the seafloor well below the base of the evaporites. Owing to the wrenching of the crustal segments which are bounded by deep-rooted fault lines like the Damietta–Latakia, Pelusium and Shelf Edge Hinge line the setting is transpressional south of 32°N, where the fault lines bend further towards the west. This adds a component of 'thick-skinned' transpression to the generally 'thin-skinned' compressional regime in the basin. Above 1.5 km of evaporites, a mud volcano is observed with the mud source seemingly within the evaporite layer. At the eastern Cyprus Arc, the convergence zone of the African and the Anatolian plates, deep-rooted compression heavily deformed the base of the evaporites, whereas at the Eratosthenes Seamount mainly superficial compression affecting the Post-Messinian sediments and the top of the evaporites is observed.

Keywords: Levantine Basin; salt tectonics; Messinian evaporites; slump; mud volcano; reflection seismic data

* Corresponding author. Tel.: +49 40 42838 5045; fax: +49 40 42838 5441.
E-mail addresses: netzeband@dkrz.de (G.L. Netzeband), huebscher@dkrz.de (C.P. Hübscher), gajewski@dkrz.de (D. Gajewski).
[1] Tel.: +49 40 42838 5184; fax: +49 40 42838 5441.
[2] Tel.: +49 40 42838 2975; fax: +49 40 42838 5441.

0025-3227/$ - see front matter © 2006 Elsevier B.V. All rights reserved.
doi:10.1016/j.margeo.2006.05.004

1. Introduction

During the Messinian Salinity Crisis, 5.9–5.3 Ma ago, thick evaporite layers were deposited in the main basins of the entire Mediterranean Sea (Hsü et al., 1973). The Messinian evaporites were the target of two DSDP legs (Hsü et al., 1973, 1978) and a number of other studies (e.g. Cohen, 1993; Clauzon et al. 1996; Gradmann et al., 2005). The evaporite facies are differentiated in basinal and marginal evaporites (Garfunkel and Almagor, 1984; Cohen, 1993; Gradmann et al., 2005). The marginal evaporites, mainly consisting of gypsum, anhydrite, carbonates and intercalated shales, are known from offshore and onshore drillings in Messinian and Pre-Messinian drainage channels (Gvirtzman and Buchbinder, 1978; Garfunkel et al., 1979; Druckman et al., 1995). The basinal evaporites presumably consist mainly of halite (e.g. Cohen, 1993). Drilling into these basinal facies did not reach the halite layer, but only an upper evaporitic layer with several tens of meters of carbonates and gypsum interspersed with Nile sediments. The reflection marking the bottom of the Messinian evaporites has been termed N-reflection and that marking the bottom of the Pliocene–Quaternary overburden has been termed M-reflection (Ryan et al., 1970).

Salt tectonics as described by e.g. Letouzey et al. (1995) and Waltham (1997) can be studied at the initial stages, because of the comparatively young age of the evaporites and because of little tectonic overprint. Gradmann et al. (2005) investigated Post-Messinian deformation in the basin in E–W direction off northern Israel. In this study we analyse the interrelation between thick-skinned tectonics, differential sediment load and subsidence, and salt tectonics in the entire Levantine Basin. This includes a discussion of the impact of the sediment load of the Nile Fan on north–south directed gravity gliding and of the importance of the Eratosthenes Seamount as a potential backstop.

2. Regional setting

The Levantine Basin lies in the south-eastern Mediterranean Sea and is considered to be a relic of the Mesozoic Neo–Tethys Ocean (Robertson and Dixon, 1984; Garfunkel, 2004). It opened during several rifting stages in the Triassic (Garfunkel, 1998; Robertson, 1998). Whether the crust underneath the basin is of oceanic origin or stretched continental crust has been a matter of debate for many decades (e.g. Woodside, 1977; Makris et al., 1983; Dercourt et al., 1986; Hirsch et al., 1995; Ben-Avraham et al., 2002), but recent studies indicate that the crust in the Levantine Basin is of continental origin (Vidal et al., 2000a; Gardosh and Druckmann, in press; Netzeband et al., 2006).

This area represents a very complex tectonic environment, which includes the northward moving African plate, the postulated Sinai sub-plate (Almagor, 1993; Mascle et al., 2000), the N–NW moving Arabian plate, and the westward moving Anatolian plate (Fig. 1).

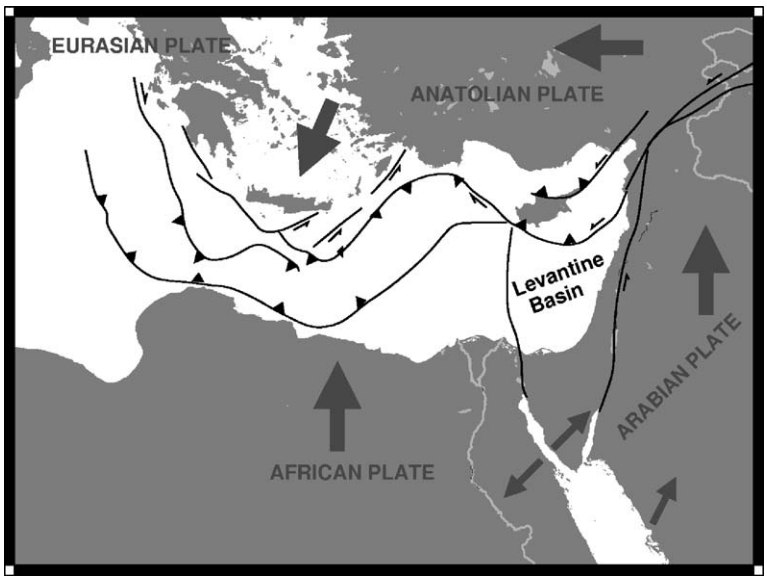

Fig. 1. Simplified tectonic map of the Eastern Mediterranean Sea. Arrows indicate the sense of plate motion, half arrows indicate transform/strike-slip faults.

The rotational movement of the Anatolian plate is accommodated by dextral strike-slip along the North Anatolian Transform Fault and corresponding sinistral strike-slip on the East Anatolian Transform Fault (Hall et al., 2005). The convergence rate of the African and the Eurasian plates in the Levantine Basin is approx. 1 cm/yr (Kempler and Garfunkel, 1994; Jiménez-Munt et al., 2003). According to Vidal et al. (2000b) the Cyprian Arc represents the current plate boundary between the African and Anatolian plates. They find that the African–Anatolian plate boundary is not a sharp boundary but a wide zone bounded by two strike slip fault systems. Ben-Avraham et al. (1995) and Woodside et al. (2002) describe the plate boundary as more or less sutured and associate it with a wrench fault system stretching from Cyprus to Syria. The lack of strong earthquakes of intermediate depth at the Cyprus Arc indicates that subduction stopped there, and the plate movement supposedly has a large transverse component (Papazachos and Papaioannou, 1999). Woodside (1977) and Hall et al. (2005) suggested that subduction at the Cyprus Arc has stopped relatively recently and has been replaced by another deformation process, because all oceanic crust has been subducted and the continental part of the African plate now meets the Anatolian Plate. According to Hall et al. (2005) the deformation at the eastern Cyprus Arc changed from compression to strike-slip after the Messinian.

Apart from the Cyprus Arc, which marks the plate boundary between the Anatolian and the African, and the Dead Sea Transform fault, which divides the Arabian and the African plates, a number of smaller fault zones has been identified in the Levantine Basin (Fig. 2). Several SW–NE striking shear zones converge

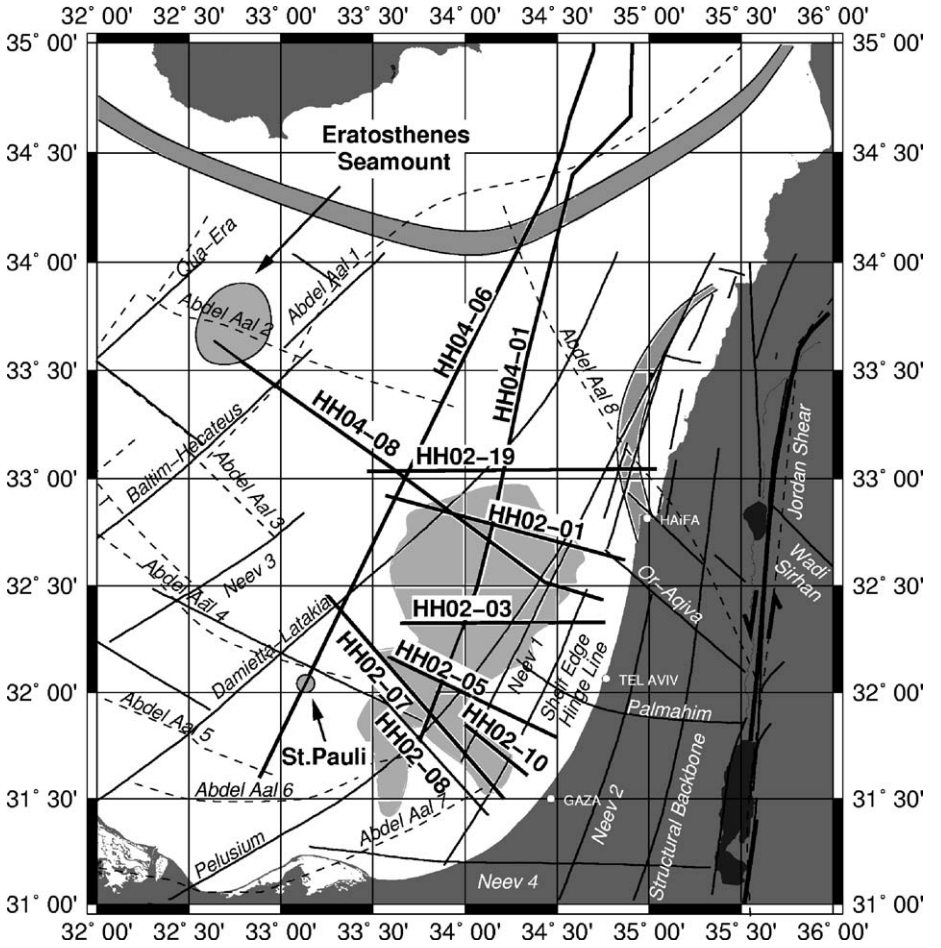

Fig. 2. Map of the study area. The Eratosthenes Seamount and the St. Pauli mud volcano are marked. Thick, solid lines indicate main seismic profiles. Thin solid lines and dashed lines represent fault lines postulated by Neev (1975, 1977), Neev et al. (1976), and Abdel Aal et al. (2000), respectively. Fault lines are labelled with their names, unnamed faults are numbered. The fault zone off Haifa after Schattner et al. (submitted for publication) and the Cyprus Arc are indicated by grey shaded arcs. The area shaded in a lighter grey corresponds to the slump complex delineated by Frey-Martinez et al. (2005).

towards the north, e.g., the Pelusium Line, the Hinge Line and the Damietta–Latakia Line (Neev, 1975; Neev et al., 1976; Neev, 1977; Abdel Aal et al., 2000). These authors also depicted NW–SE trending fault lines. Mart (1984) confirmed these findings and suggested that the NNE–SSW directed faults are normal faults, and the NW–SE oriented faults are strike-slip faults and possibly originate in the crust. According to Neev (1975), the north-eastward wedging compressional features originate in the south-eastern corner of the Mediterranean, although no evidences have been presented. Abdel Aal et al. (2000) also showed faults trending NNE–SSW and NW–SE which more or less coincide with the fault lines depicted by Neev et al. (1976) (Fig. 2).

The Pelusium line represents the western edge of the Syrian Arc fold belt. According to Gardosh and Druckmann (in press) the evolution of this regional compressional tectonic feature started in the Late Cretaceous and persisted until the Early-Middle Miocene. Its evolution was related to the closure of the Neo-Tethys (see Garfunkel, 1998, 2004 for comprehensive summaries). Gradmann et al. (2005) interpreted seismic data off northern Israel and suggested tectonic activity along the shear-zones also in the Pliocene–Quaternary. North of Haifa, the converging shear zones merge with the seismically active Carmel fault zone, which continues along the central Levantine continental margin, viz from the Carmel Structure in the south until south of Beirut (Schattner et al., submitted for publication) (Fig. 2). In the following discussions, we consider the Pelusium line as a regional tectonic feature in the south-eastern Mediterranean and not as a transcontinental shear as proposed by Neev (1977).

The sediment fill of the Levantine Basin reaches a thickness of up to 14 km (Ben-Avraham et al., 2002; Netzeband et al., 2006). It is composed of a carbonate layer of possibly Cretaceous to Jurassic age with a thickness of 1–3 km, followed by several km of Paleogene–Neogene pelagic sediments, a layer of Messinian evaporites of up to 2 km thickness, and a Pliocene–Quaternary cover, which mainly consists of the Nile sediments (Druckman et al., 1995; Vidal et al., 2000b; Ben-Avraham et al., 2002; Ben-Gai et al., 2005). The Messinian evaporites were deposited during the Messinian Salinity Crisis, when the evolving Mediterranean Sea lost its connection to the Atlantic, mainly because of the collision of the African and Eurasian plates (Hsü et al., 1973, 1978). The blocked water exchange and the high evaporation rate caused a drop in sea level, an increase in salt concentration and finally precipitation of evaporites. Druckman et al. (1995) estimated the fall of the sea level to approx. 660–820 m, Ben-Gai et al. (2005) found evidence of a sea level fall of 800–1300 m. As a consequence, the Mediterranean Sea was a succession of more or less separate basins with different rates of sedimentation and different depositional environments (Montadert et al., 1978). According to Hsü et al. (1973), the reflooding was a very rapid event, lasting only 1000–2000 yrs. Rouchy and Saint Martin (1992) estimated that about 25 cycles of refill and subsequent drawdown or a semi-permanent inflow of fresh water or a combination of both are required to deposit the amount of evaporites found in the basins in the Mediterranean Sea. Whereas Hsü et al. (1978) only acknowledged one single transparent evaporite layer, Rouchy and Saint Martin (1992) assessed from borehole analysis in the Western Mediterranean Sea that basinal evaporites generally consist of 2 successive units, one consisting of massive chloride salt and the other of calcium sulphate–marlstone interbedded with rare chloride salts. Polonia et al. (2002) observed even 4 subunits of Messinian evaporites in the Herodotus Abyssal Plain southwest of Cyprus. Bridge et al. (2005) found probably non-halitic units within the evaporite succession in the Cilicia Basin north-east of Cyprus, and Gradmann et al. (2005) also found prominent internal reflections within the evaporite layer in the Levantine Basin. Garfunkel and Almagor (1984) and Garfunkel (1984) offered an interpretation of such internal reflections as embeddings of over-pressurized clastic sediments between evaporites. The Nile Scarp, an up 600 m high escarpment lies south and east of the Eratosthenes Seamount (Abdel Aal et al., 2000), which is considered to be the backstop of the compressed Messinian evaporites.

The deposition of the Pliocene–Quaternary sediments above the Messinian evaporites is determined by the sediment supply of the Nile River (e.g. Mart and Ben-Gai, 1982). The thickness of the sediment cover and the sedimentation rate decrease accordingly to the north, a sedimentation rate of 162 m/Ma in Echo-1 (near HH02-05, <50 m water depth) and 111 m/Ma in borehole Delta-1 (near line HH02-03 (Fig. 2) in about 120 m water depth) are given for the Pleistocene by Tibor et al. (1992). According to Tibor and Ben-Avraham (2005), the Levantine Basin becomes shallower, because sedimentation exceeds subsidence. After anomalously high subsidence rates in the Pliocene (123 m/Ma in Echo-1) as a flexural response to the rapid deposition of Messinian evaporites, the subsidence was significantly reduced (7 m/Ma in

Holocene in Echo-1) (Tibor et al., 1992; Ben-Gai et al., 2005). The entire subsidence of the top of the Messinian amounts to 500 m in the basin (Tibor et al., 1992).

Several slumping complexes were found offshore Israel (Garfunkel, 1984; Mart, 1987; Almagor, 1993; Frey-Martinez et al., 2005). Almagor (1984, 1993) found seismic evidence of displaced sediments along the entire slope offshore Israel, and classified earthquake triggered slumping as the most important agent of downslope sediment transport. Based on the analysis of an extensive 3D dataset, Frey-Martinez et al. (2005) found over 40 slump complexes within the Post-Messinian, seismically characterized by a zone of chaotic or weak reflections appearing almost transparent. Three stratigraphic units are identified, which show different slumping behaviour. The Holocene shows numerous (about 25) small slump bodies, with no more than 80 km^3, in the Pleistocene approx. 15 slump bodies have been found with a size of 400 km^3, and in the Pliocene one single slump complex has been detected, the Israeli Slump Complex (ISC). According to Frey-Martinez et al. (2005), the ISC consists of at least three major slumps accounting for 1000 km^3, effecting an area of 4800 km^2, which places the ISC in the dimension of the Storegga Slide offshore Norway.

Mud volcanoes are found in several places in the Eastern Mediterranean Sea, mainly on the Mediterranean Ridge (Huguen et al., 2005), at the Anaximander Seamount (Dimitrov and Woodside, 2003) and in the Nile Deep Sea Fan (Loncke et al., 2004). They usually occur in clusters, accompanied by pockmarks (Dimitrov and Woodside, 2003). Pockmark fields without neighbouring mud volcanoes are furthermore found on the top of the Eratosthenes Seamount (Dimitrov and Woodside, 2003) and in the southeastern Levantine Basin (Coleman and Ballard, 2001).

3. Materials and methods

The data of this study were collected during the GEMME cruise M52/2 (HH02-lines) with the German research vessel *RV METEOR* in 2002 (Pätzold et al., 2003) and during the SAGA expedition (cruise PE228; HH04-lines) with the Dutch research vessel *RV PELAGIA*. 44 multi-channel seismic reflection lines were recorded during the cruise M52/2, and another 12 reflection lines were recorded during the cruise PE228 (Figs. 2 and 3a). All were recorded with a streamer of 600 m active length. Profiles HH02-01, HH02-03, HH02-05, and HH02-08 were also recorded with a second streamer of 150 m active length. Both streamers comprised 24 channels with a group distance of 6.25 m and 25 m, and a maximum offset of 190 m, and 700 m, respectively. Both recorded with a sampling rate of 1 ms. For HH02-07 and HH02-19 the source consisted of two airgun small clusters: one with two GI-Guns, each with a volume of 105 $in.^3$ operated in the harmonic mode, and the other cluster consisting of one GI-Gun with 205/105 $in.^3$ operated in the airgun mode and a G-Gun of 380 $in.^3$ (6 l). For HH02-01, HH02-03, and HH02-05 only the GI-Gun cluster ($2\times205/105$ $in.^3$) was used, and for HH04-01, HH04-06, and HH04-08 the source consisted of 2 G-Guns with 380 $in.^3$ (6 l) each. The shot spacing was 25 m (10 s).

The recordings of both streamers were CMP-sorted with a CMP spacing of 6.25 m and 12.5 m, then stacked and bandpass filtered with passing frequencies between 10 and 150 Hz. On lines HH02-07, HH02-19, HH04-06, and HH04-08 further processing was applied on the recording of the longer streamer:

- a stacking velocity analysis on every 100th CMP in supergathers of 5–9 CMPs. The deeper the analysed horizon, the more CMPs in the supergather.
- smoothing or the resulting velocity field
- time-migration and stacking
- interval velocity analysis
- model based pre-stack depth migration.

Interval velocities of Post-Messinian sediments and evaporite layers were 2.0 ± 0.2 km/s and 4.2 ± 0.3 km/s. With a maximum offset of 800 m and the base of the evaporites at ~4 km, the interval velocity of the evaporite layer was difficult to determine, and it was impossible to find any reliable interval velocity from below.

We carried out an Airy-backstripping of the Pliocene–Quaternary sediments after Allen and Allen (1990). We simply removed the sediment load, not taking into account any effect of compaction of either evaporites or Pre-Messinian sediments. The relation of the depth of the present seafloor and the seafloor after backstripping is given in Eq. (1).

$$d_{\text{seafloor}} = d_{\text{w}} + d_{\text{sed}}(\rho_{\text{mantle}}-\rho_{\text{sed}})/(\rho_{\text{mantle}}-\rho_{\text{w}}) \qquad (1)$$

Here, d_{seafloor} denotes the depth of the seafloor after backstripping, d_{w} denotes the present water depth and d_{sed} the thickness of the sediment layer that is removed. ρ_{sed} marks the density of the sediment layer, ρ_{w} the density of the water column and ρ_{mantle} the density of

the mantle. For ρ_w, ρ_{sed}, and ρ_{mantle} we assumed densities of 1.03 g/cm^3, 2.0 g/cm^3 and 3.3 g/cm^3, respectively, for the evaporites 2.2 g/cm^3. (Ben-Avraham et al., 2002; Netzeband et al., 2006). We also applied this method with the same parameters to the backstripping of individual evaporite layers.

4. Results

Top (M) and base (N) of the evaporite layer are clearly visible on all seismic lines. As an overview, a rough map of Pliocene–Quaternary sediment thickness and evaporite thickness in the southern portion of the

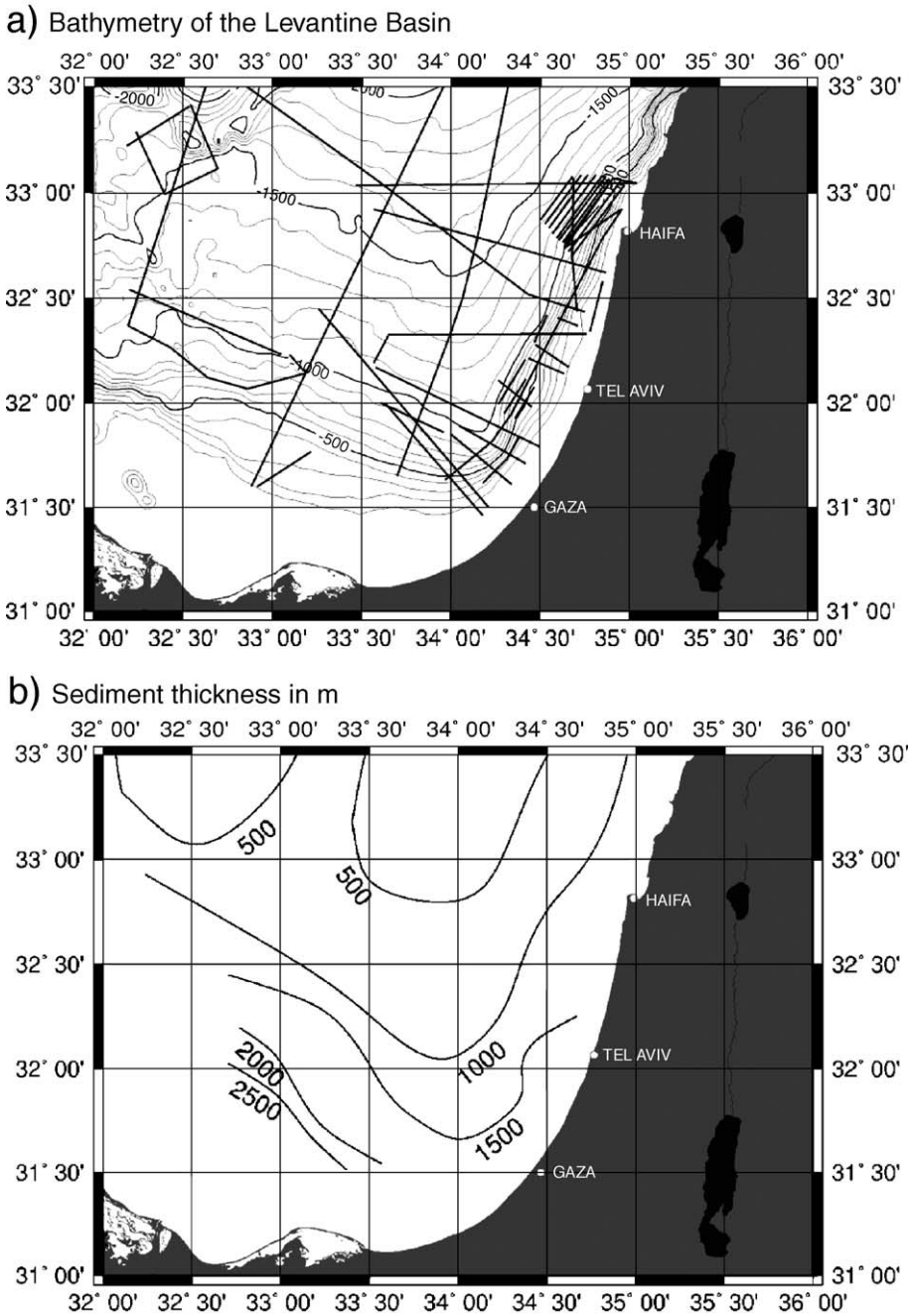

Fig. 3. Maps of study area: a) bathymetry of the Levantine Basin, numbers correspond to depth in m. All the seismic lines this study is based on are shown for reference. Note the Eratosthenes Seamount south of Cyprus. b) isolines indicating the sediment thickness in the Levantine Basin. c) isolines indicating the thickness of the evaporite body in the Levantine Basin.

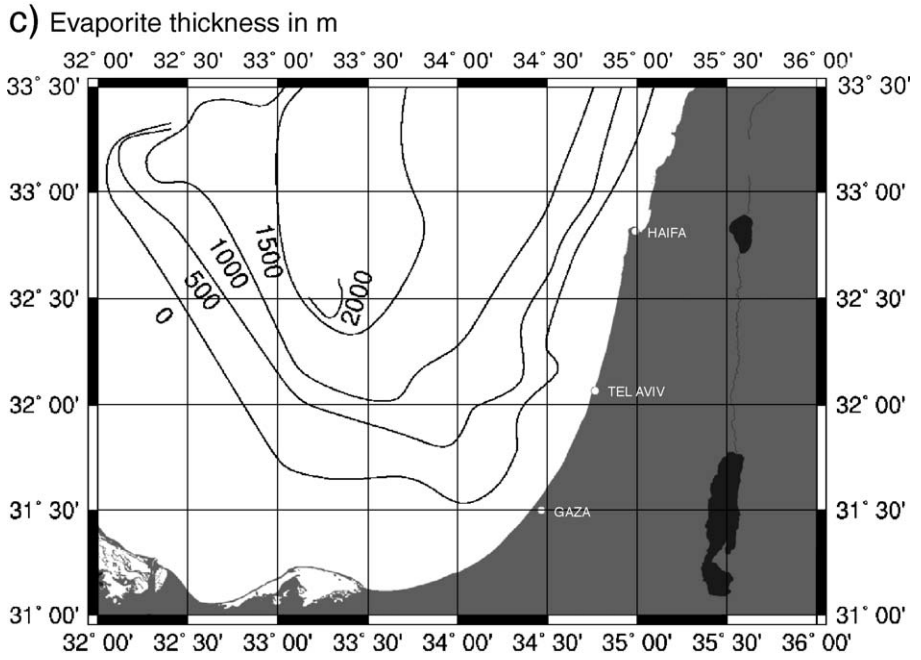

Fig. 3 (*continued*).

Levantine Basin is shown in Fig. 3b and c, line drawings of depth migrated lines HH04-06 and HH04-08 are shown in Fig. 4a–d. On the slope of the Nile Delta the Pliocene–Quaternary sediment thickness reaches thicknesses of almost 3 km, while in the centre of the basin the thickness is less than 500 m. The sedimentary cover is also reduced around the Eratosthenes Seamount (Fig. 3b).

The thickness of the Messinian evaporites, in contrast, increases towards the centre of the basin to over 2 km (Fig. 3c). The evaporites extend to about 30 km off the Israeli coast, the boundary runs more or less parallel to the coast. This distribution reveals the NNE–SSW orientation of the Levantine Basin, which is also indicated by the bathymetry (Fig. 3a).

4.1. Post-Messinian subsidence

All seismic lines show a thinning of the basinal evaporites towards the eastern and southern margin of the basin (Fig. 4a, b). The top of the evaporites, the M-reflection, declines towards the pinchout and forms an apparent rollback anticline. A typical example of such a rollback on W–E striking lines is presented in Fig. 5. Besides the rollback, these lines show a group of faults close to the pinchout. The subsidence analysis aims at the explanation of the rollback in terms of lateral gravity gliding or differential subsidence. After backstripping of the Pliocene–Quaternary sediment layer, the top of the evaporites is basically flat and horizontal, except for some small-scale undulations (Fig. 6). This result is in accordance with the results of Tibor and Ben-Avraham (2005), who performed 2D-backstripping including decompaction. Line HH02-01 south of Haifa is the only significant exception. Here, the presence of salt rollers and salt welds proves lateral salt withdrawal (see Gradmann et al., 2005, for a comprehensive discussion).

The removed Pliocene–Quaternary sediment layer is of more or less constant thickness along the Israeli margin, with about 500 m in the basin and 1.1 km at the shelf (Fig. 6). The calculated subsidence in the basin amounts to 200 m. Differential sediment load and subsidence occurred between the upper slope and the central basin. It should also be mentioned that on the northern W–E striking lines the pinchout of the evaporites lies basinwards from shelf break, whereas in the south of HH04-06 and HH04-01 the evaporites extend under the shelf.

At the Nile Fan, in the south of line HH04-06, which is N–S oriented, nearly 3 km of sediments overlie the evaporites due to the proximity to the Nile delta. Here, the M-reflection is clearly planer after the backstripping, but the depth still varies between 1.8 and 2.4 km. Near the southern rollback, the depth of the M-reflection is about 2.1 km, going north we see forebulging with the M-reflection rising for approx. 80 km to only 1.8 km

depth and then declining again towards the centre of the basin to 2.4 km.

4.2. Internal reflections

Up to 4 internal reflections (E1–E4) are observed within the evaporite layer with varying reflection and deformation patterns (Figs. 4 and 7). These mostly well pronounced reflections separate seismically transparent sequences. E1 shows similar reflection characteristics as the N-reflection, and the reflection characteristics of E2 and E3 also resemble each other and those of E4 and the M-reflection as well. The thickness of the internal sequences is more or less constant with 0.2–0.4 km in the basin, leading to a total evaporite thickness of approx. 1.6 km.

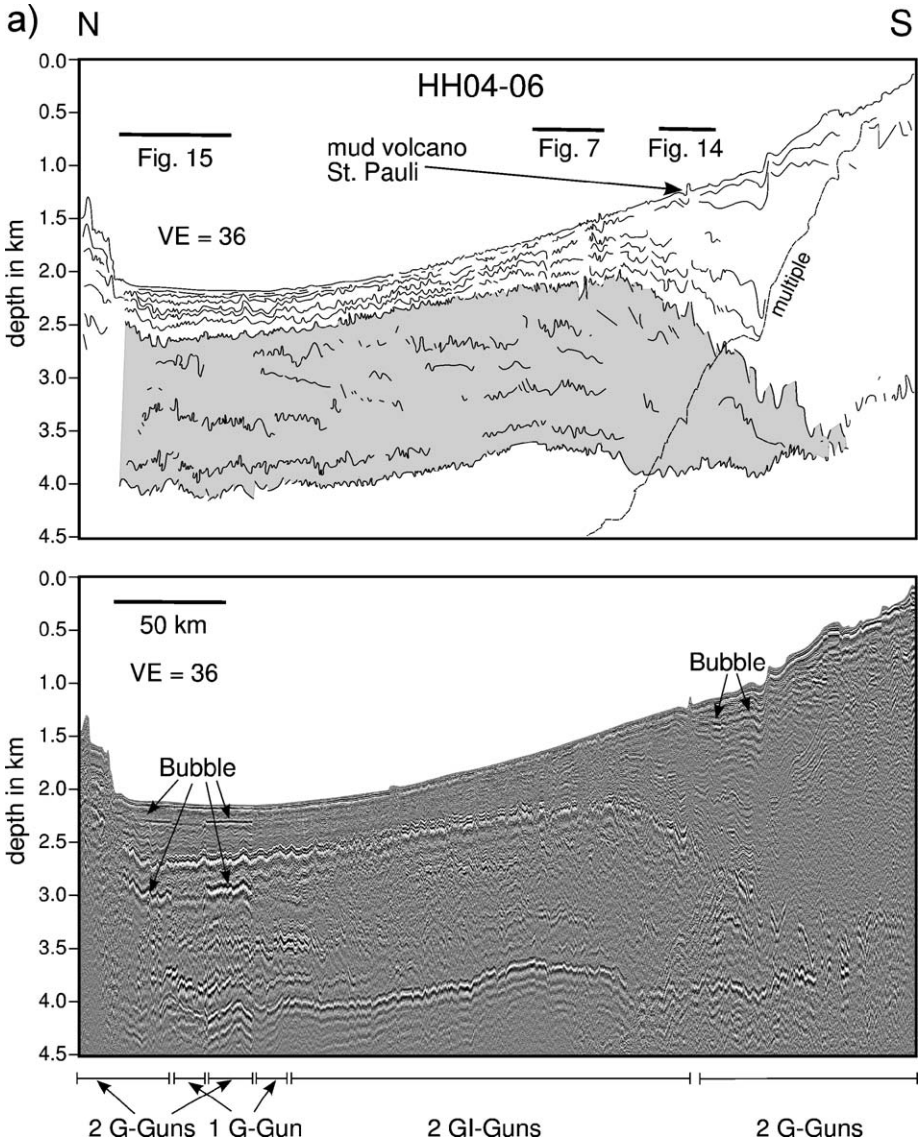

Fig. 4. (a) Depth migrated seismic line (below) and line drawing (above) of line HH04-06. The seafloor multiple is marked by the dashed line, the grey shaded area indicates the evaporite layer. Internal reflections within the evaporite layer are observed. The forebulging of the evaporite body is clearly visible. (b) Depth migrated seismic line (below) and line drawing (above) of line HH04-08, analogue to (a). The grey shaded area indicates the evaporite layer. Internal reflections within the evaporite layer are observed. The positions of the major fault lines (Baltim-Hecateus, Damietta-Latakia, Pelusium, Neev 1 fault line, and the Shelf Edge Hinge line) are marked. (c) and (d) simplified line drawings of lines HH04-06 (c) and HH04-08 (d). The grey areas mark the evaporite body, M and N correspond to top and bottom of the evaporites, respectively. The solid lines labelled E1–E4 indicate the observed internal reflections, the dashed lines indicate extrapolation, where the internal reflections are not clearly visible.

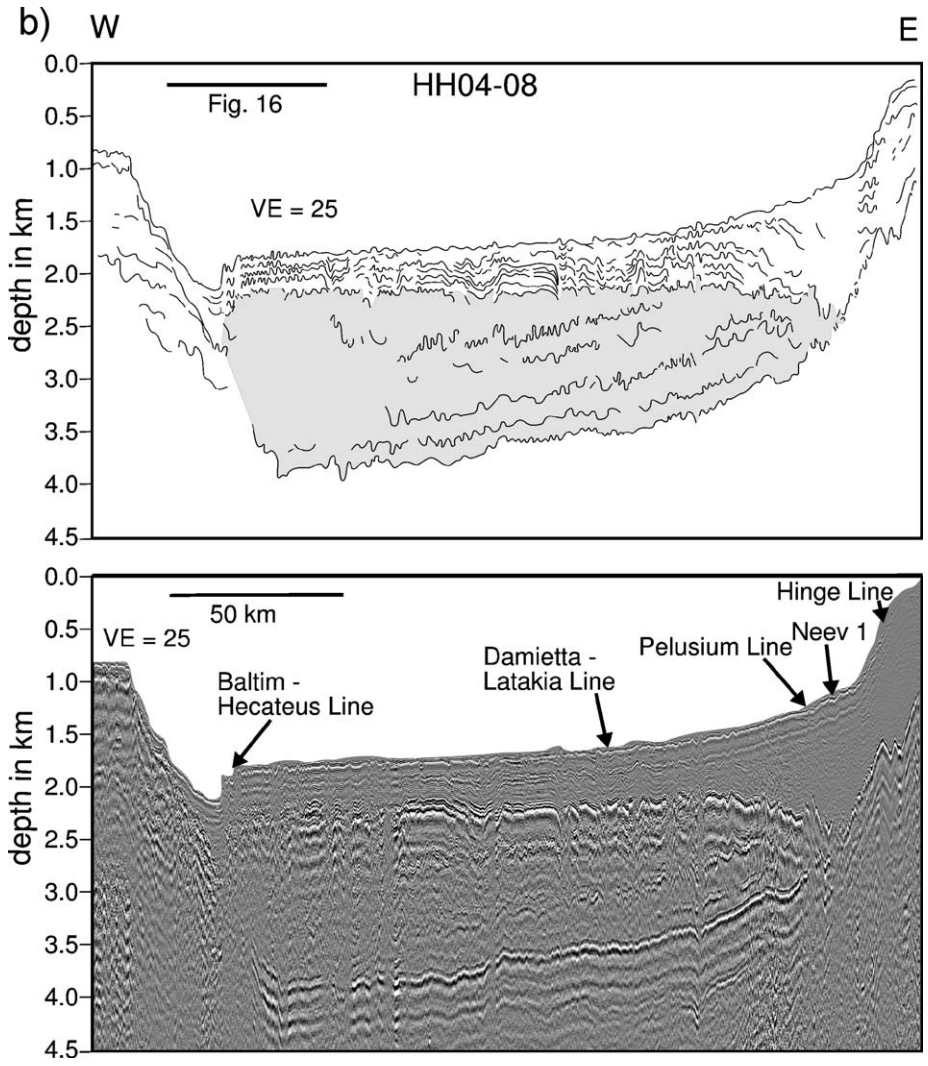

Fig. 4 (*continued*).

On the N–S profiles, e.g. HH04-06 (Figs. 4a, and 7), the deformations of these internal reflections and of the M- and N-reflections do not necessarily correspond with each other. Different kinds of deformations can be observed at the same location in different layers (Fig. 7, CMP 23200, CMP 23600, CMP 24100). One of the steepest thrusts observed in E4 is visible at CMP 23500 on line HH04-06 (Fig. 7), while the M-reflection and the seafloor above are not affected and the overburden overlies the M-reflection concordantly. The maximum thrust angle of the internal reflections is highest in E4 and decreases with depth. In E4 on line HH04-06 thrust angles of 8° are observed, up to 14° are reached at the tip of the thrusts (Fig. 7). On N–S lines, the general orientation of thrust faults and oblique folds within the evaporites is northward, i.e. basinwards, on line HH04-01 and HH04-06 (Figs. 2, 4a, and 7)). On N–S lines, E1–E4 are only parallel to the basal N-reflection in the northern part, but they seem to downlap onto the N-reflection beneath the Nile Fan and near the pinchout of the evaporites (Fig. 4a, c).

Typically, on E–W lines all internal reflections dip basinward and run parallel to basal N-reflection (Fig. 4b, d). Here, the evaporite thrusts are only observed in the top of the evaporites and E4, e.g. in lines HH02-01 (Figs. 2 and 8), HH02-03 and HH04-08 (Figs. 2 and 4b). Both eastward and westward oriented thrusts and also pop-up structures are observed (Fig. 8). Strongly folded intra-evaporite reflections are also present. In general, on the lines running E–W thrusting is less pronounced within the evaporites than on those running N–S.

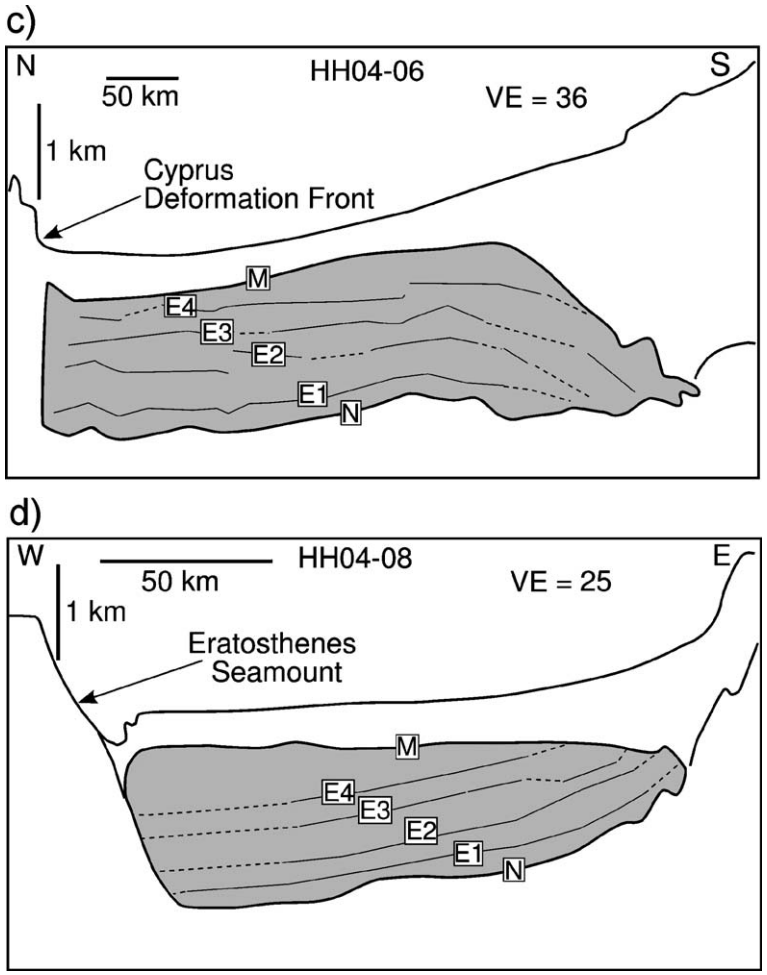

Fig. 4 (*continued*).

In order to explain the basinward dipping internal reflections we performed backstripping of the internal sequences from top to bottom of line HH04-08 (Fig. 9a–g). The tops of the individual evaporitic sequences are not horizontal after backstripping the overburden, but still dipping westwards. No basinal evaporites are deposited at a depth less than 1800 m. At the eastern edge, the evaporites prograde towards the basin. After removal of the lowermost layer, the basin remains asymmetric. On the assumption that each layer was horizontally deposited, we removed the tilt of the basin at 180 km after backstripping the Pliocene–Quaternary and the uppermost evaporitic sequence until the top of the evaporites was horizontal (Fig. 9h). Consequently, the deeper sequences became also almost horizontal (Fig. 9 h–l). After backstripping the remaining evaporitic sequences the basin is approx. symmetric between Eratosthenes Seamount and the Israeli slope.

4.3. Marginal structures

The eastern basin margin off Israel is characterized by extensional faulting. Listric and antithetic growth faults, sometimes forming keystone grabens, are observed along the entire slope (Figs. 10 and 11). Some of these faults can be traced from the seafloor to the top of the evaporites, some even penetrate the base of the evaporites. They occur where the thickness of the evaporite layer decreases towards the slope to less than 1 km. In these locations the top and the base of the evaporites are heavily faulted and folded and difficult to trace. Active extensional faults which are piercing the seafloor are also observed on the Nile Fan. Mapping these faults and keystone grabens as extensional features reveals that the extensional regime prevails in a narrow corridor parallel to the coastlines (Fig. 12).

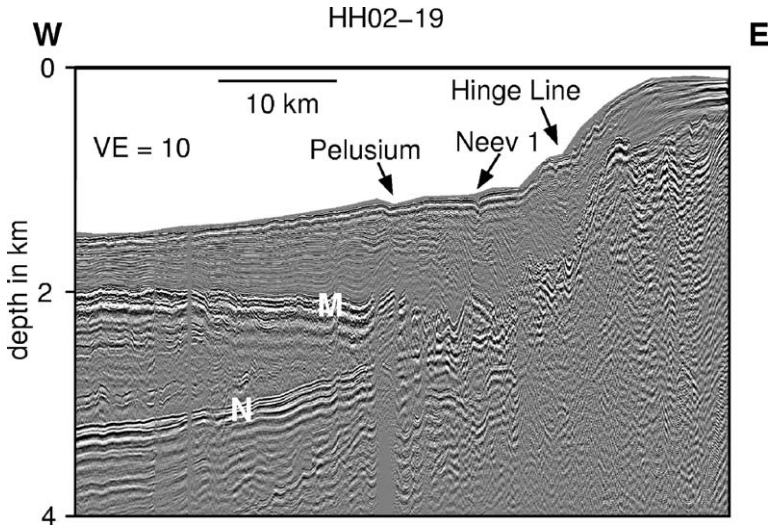

Fig. 5. Section of seismic lines HH02-19, showing the pinchout of the evaporite layer and the apparent rollback. Top and bottom of the evaporites are marked M and N, respectively. Note the decline of the M-reflection towards the pinchout. The position of the major fault lines (Pelusium, Neev 1 Fault Line, and the Shelf Edge Hinge Line) are marked.

According to the tectonic maps of Neev (e.g. 1975), several shear-zones termed Pelusium, Neev1 and Shelf Edge Hinge Lines narrow towards the north. On line HH02-03 both the entire evaporitic succession and the overburden are disrupted and the associated faults within the PQ pierce the seafloor (Fig. 13). The location of the Hinge Line is also accompanied by seafloor piercing faults and a significant change in the slope angle of the Pre-Messinian. Further south, e.g. on line HH02-10, the Shelf Edge Hinge Line is represented by the divergent reflection pattern of a divergent growth fault within the PQ, which is covered by mass waste deposits (Fig. 10). Displacements of individual growth faults reach values of up to 300 ms TWT (>220 m). The evaporitic succession is dissected. However, there is no indication of differential subsidence at both sides of the fault or of lateral salt withdrawal and creep. Since the slope angle decreases from north to south, the impact of the Hinge Line is less pronounced in the Pliocene–Quaternary sediment layer south of 32°.

The Pelusium Line and the Syrian Arc change their striking directions from NNE to NE south of 32°N. Here, the Pelusium- and Neev1 Lines are characterized by an intricate fault system. On line HH02-08 (Fig. 11), the M- and N-reflections are pretty much blurred by the multiple, especially on the western half. However, an apparently 10 km wide and at least 400 m high (500 ms TWT, Vp>1.6 km/s) anticline can be clearly identified at the top of the Pre-Messinian. Basinwards, this unconformity forms 10 km wide and south-eastward tilted terraces. Above the dominant anticline the Pliocene–Quaternary shows a vertical succession of sequences, some of which are of laterally equal thickness and some are thinned above the crest. On the north-western flank a segment with divergent reflections (listric growth faults) follows. An uplifted horst is framed by two graben-like features. Most of the faults pierce the seafloor. In accordance with Neev (1975), the anticline corresponds to the Neev1 line, while the horst and the western graben correlate with the Pelusium Line. In general, all major fault lines can be identified in the available seismic data off Israel.

4.4. Israeli Slump Complex

The ISC can be identified on lines HH02-03, HH02-05, HH02-01, HH02-19, HH02-07, and HH04-08 (e.g. Figs. 10 and 13). This zone of heavily disturbed sediments is almost seismically transparent, whereas the sediments above and below are well stratified. The ISC is prominent on the slope where it reaches a thickness of up to 200 m at a depth of 150–250 m below seafloor (bsf), and then thins towards the basin. There it can be correlated with a seismically transparent sequence that is present throughout the basin, also in the Nile Fan and serves as an isochrone. This transparent sequence shows a more or less constant thickness of approx. 50 m in the basin, whereas the zone of disturbed sediments near the shelf significantly varies in thickness.

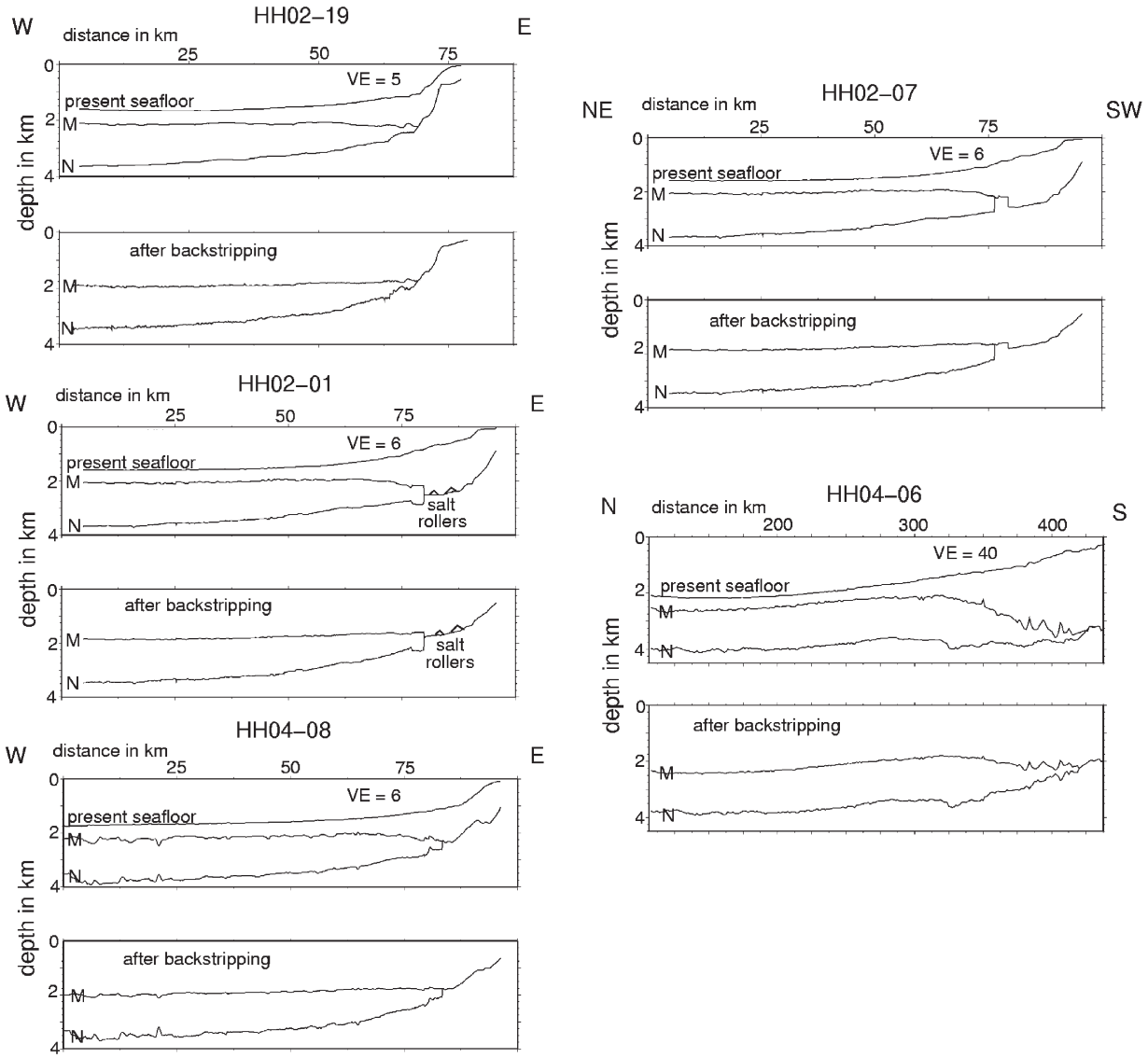

Fig. 6. Examples of airy backstripping. Sketches of several profiles split into two parts: the present seafloor, top and bottom of the evaporites in the upper part, and top and bottom of the evaporite layer after backstripping of the Pliocene–Quaternary sediments in the lower part. Vertical exaggeration (VE) varies.

4.5. Mud volcano

A mud volcano is observed at CMP 28000 (33°20 E/32°20 N) on the southern part of Line HH04-06 (see Fig. 2), which we named 'St.Pauli' (Fig. 14). This mud volcano lies at a water depth of 1.2 km and approx. 150 km offshore Egypt. It rises to 120 m above the seafloor and has an apparent width of over 1.5 km. The overburden beneath is severely distorted and a caldera-like feature underlies the mud volcano approx. 300 m beneath the seafloor.

The uppermost evaporitic sequence beneath forms a cone-like structure with an apparent width of 4 km. Several strong intra-salinar reflections pinch out against this cone. It is unclear to which extent deeper reflections are affected, because they are partly concealed by the seafloor multiple. However, the continuous base of the evaporites, the N-reflection, can be clearly identified. The entire evaporitic sequence beneath St. Pauli is still about 1.5 km thick. There is no evidence for any significant extension, faulting or folding, nor for salt welds.

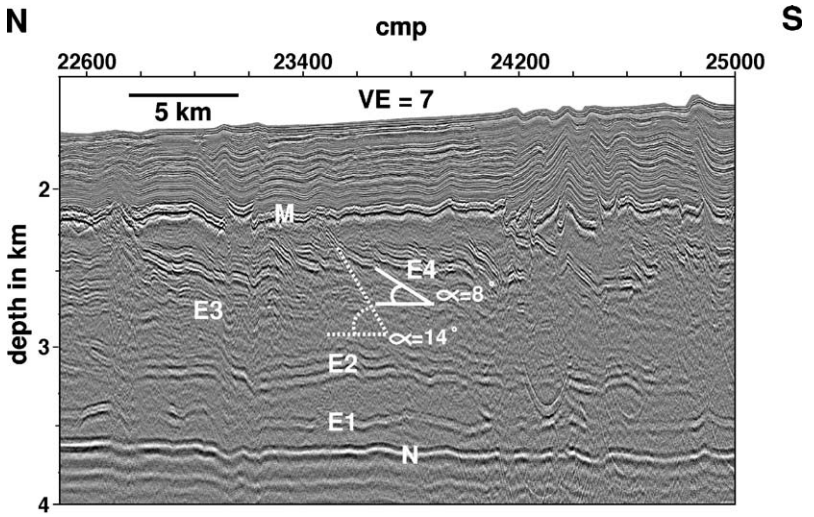

Fig. 7. Section of seismic line HH04-06, depth migrated. Top and bottom of evaporite layer are indicated by M, and N, respectively. E1–E4 mark the internal evaporite reflections. Note the large angles of thrust within the internal reflections, particularly in E4. Two angles (the solid angle corresponding to 8°, the dashed one to 14°, the vertical exaggeration is 7) are drawn for reference.

4.6. The basin

Compressional features such as folding, thrusting and pop-up structures in the basin are observed on all profiles, defining an area of compression in the centre of the basin (Fig. 12). In N–S direction thrusting prevails which is directed northwards, while in E–W direction the deformation is more symmetrical, pop-up structures are found, and thrusts are as common in eastward as in westward direction. The degree of compression varies within the evaporite layers as well as within the Pliocene–Quaternary cover (Figs. 7 and 8).

There is an abundant number of compressional faults within the basin which reach from the upper evaporites to the transparent sequence mentioned above (e.g., (Figs. 7, 8, and 13)). These faults show a constant displacement beneath the transparent layer. They can be

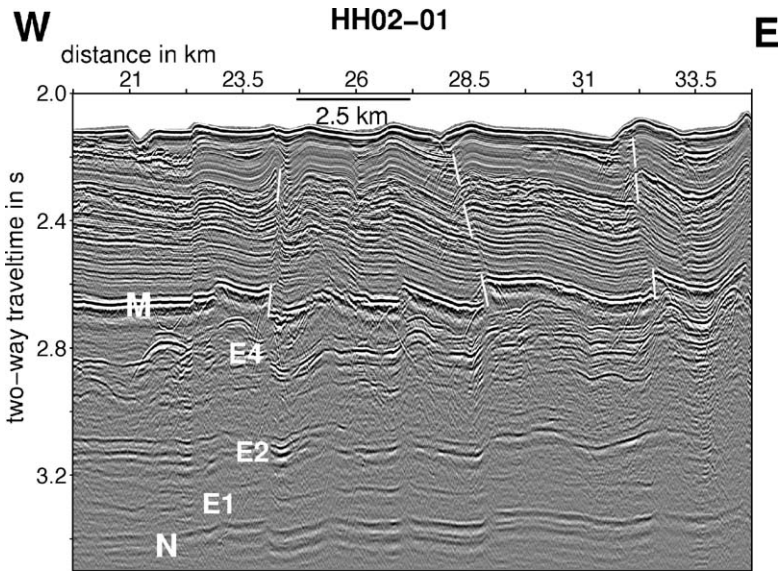

Fig. 8. Section of seismic line HH02-01, time migrated. Top and bottom of evaporite layer are indicated by M, and N, respectively. E1–E4 mark the internal evaporite reflections. Note the constant throw of the thrusts up to a certain level.

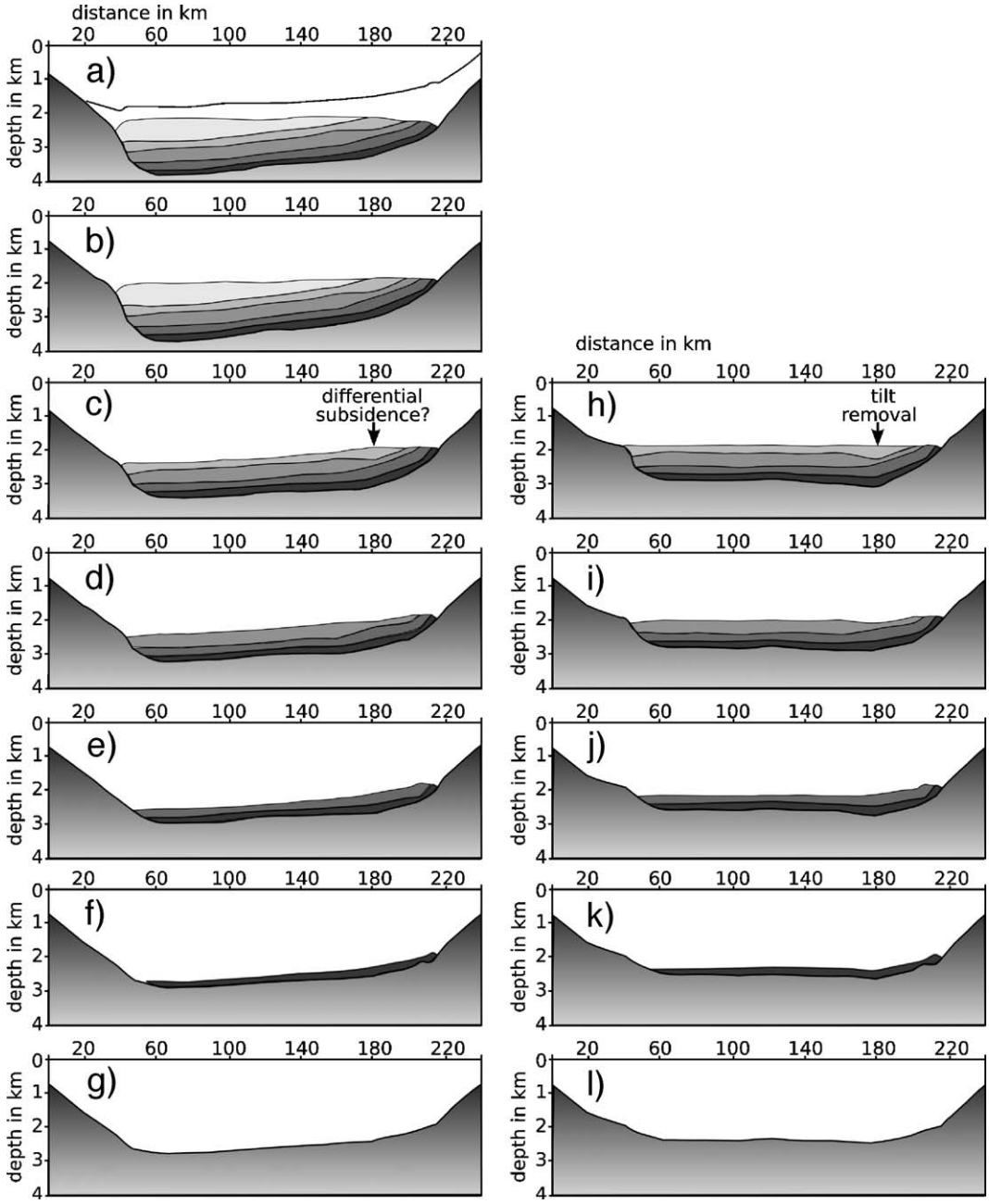

Fig. 9. Airy backstripping of line HH04-08, including the internal salt reflections. The left column, a–g represents the backstripping results, as one layer at a time is removed. The right column, h–l, shows a modification of the backstripping: After removal of the Pliocene–Quaternary and the uppermost salt layer, the basin is partially uplifted, basinwards from km 180, until the top of salt is horizontal. Then backstripping is continued.

found as far into the basin as 140 km off the ISC. Consequently, slumping and faulting are coeval processes.

The fold height and compression increase towards the Cyprus Arc. Up to 50 km south of the Cyprus Arc the base of the evaporites and the internal reflections E1 and E2 are deformed much more heavily than in the basin. The M-reflection and E4, in contrast, show accented deformation compared to the basin only for approx. 25 km, whereas the seafloor looks flat and undisturbed (Fig. 15). The lower part of the Post-Messinian sediments, a complex of

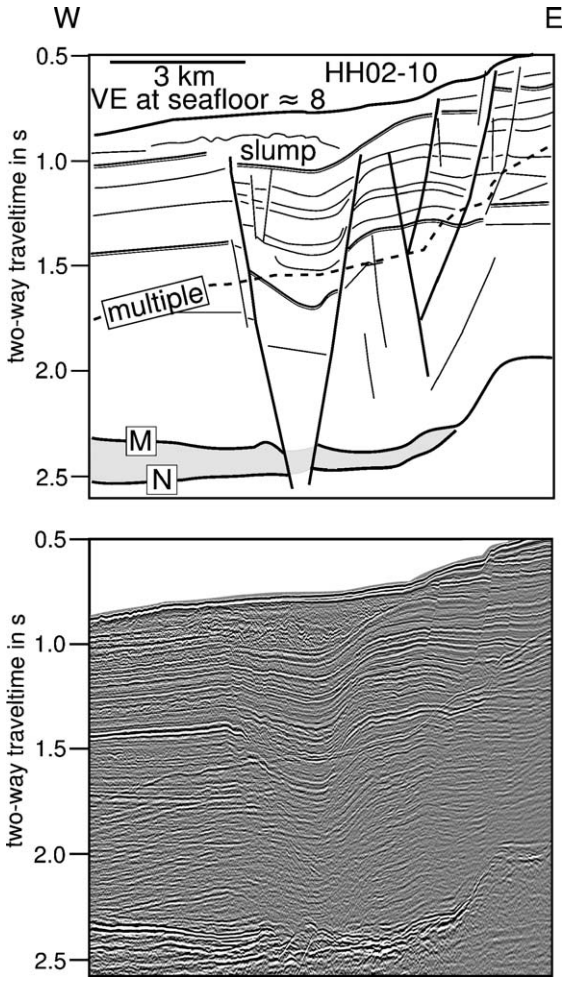

Fig. 10. Section of time migrated seismic line (below) and line drawing (above) of profile HH02-10, showing the location of the Shelf Edge Hinge line. Top and bottom of the evaporite layer are indicated by M, and N, respectively, and the seafloor multiple is marked by the dashed line. Major faults penetrate the evaporite layer, and further upslope a flower structure is expressed. Also, evidence of a slump is observed.

constant thickness of about 220 m shows the same deformation patterns as the M-reflection, indicating pre-kinematic deposition (Fig. 15). Above this pre-kinematic sediment package the deformation in the sediments decreases to about 50–100 m below the seafloor. These upper 50–100 m of sediments show no deformation at all, indicating post-kinematic deposition.

At the Eratosthenes Seamount the seafloor is heavily deformed, almost parallel to the top of the evaporites, which pinch out near CMP 3000 at the very steep angle of 23° (Fig. 16). Here the M-reflection is heavily distorted and disrupted, much in contrast to the N-reflection, which appears smooth until it begins to rise at an angle of about 4° near CMP 4300 and disappears approx. 10 km off the flank of the seamount. Internal reflections are not continuously observed, therefore it is not possible to determine down to which depths the evaporites are affected by compression. Nevertheless, the N-reflection does not seem to be affected.

5. Discussion

5.1. Origin of the internal reflections

Up to 4 internal reflections within the evaporites are observed in the Levantine Basin (Figs. 4, 7, and 8). Internal reflections and layering of evaporites in the Mediterranean Sea have been described by other authors (e.g. Réhault et al., 1984; Garfunkel, 1984; Rouchy and Saint Martin, 1992; Polonia et al., 2002; Gradmann et al., 2005; dos Reis et al., 2005). Three explanations have been given for these reflections: a) interbedded shales, b) layers of different evaporites, and c) several depositional cycles.

a) Garfunkel (1984) and Garfunkel and Almagor (1984) postulated overpressured shales interbedded within the impervious evaporites. This explanation cannot be ruled out. However, it does not explain the different deformation pattern of the individual evaporitic sequences nor their different rheology.
b) Réhault et al. (1984) identified three layers within the evaporite succession in the Western Mediterranean: upper evaporites (composed of halite, gypsum and marls), salt (halite), and lower evaporites (possibly of the same composition as the upper evaporites). dos Reis et al. (2005) found these three layers also in the Gulf of Lions. Polonia et al. (2002) detected two units within the Messinian in the Eastern Mediterranean Sea. They interpreted the upper unit, which is characterised by folded high-amplitude reflections, as upper evaporites composed of marls and gypsum, and the lower unit, which is almost transparent and reflection-free, as halite. These observations and interpretations delineate a single cycle of evaporite deposition.
c) Cohen (1993) described a typical depositional cycle of Messinian evaporites in the Levantine Basin as marine clay → gypsum → halite, although he found from well measurements that quite often one of the evaporitic members is missing and cycles become a couplet of either clay → gypsum or clay → halite. Our observation of 4 internal reflections, i.e. 5 including the M-reflection, with 5 transparent layers

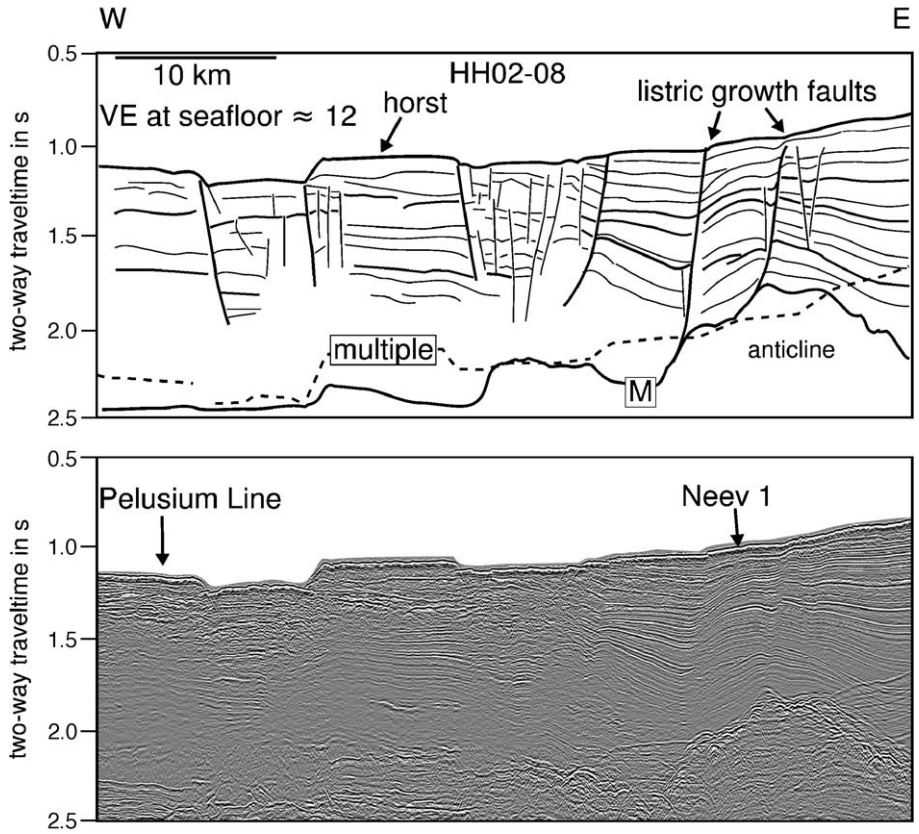

Fig. 11. Section of time migrated seismic line (below) and line drawing (above) of profile HH02-08. The top of the evaporite layer is indicated by M, and the seafloor multiple is marked by the dashed line. Note the anticline and the horst-graben structure.

in between leads to the assumption of 5 cycles of evaporite deposition. Cohen (1993) also observed several cycles of evaporites in boreholes offshore Israel. Consequently, we suggest that the single intra-salinar reflections mark the boundaries between 5 cycles of evaporite deposition. This explains also the brittle deformation of the uppermost evaporites, as already described by Gradmann et al. (2005), owing to the presence of, e.g., anhydrite or gypsum at the top of each sequence.

5.2. Syn-depositional evaporite deformation

The vertical variation of the distortion patterns of each intra-salinar reflection and evaporitic sequence, respectively, can be interpreted by syn-depositional deformation before the next sequence was deposited. The orientation of the internal reflections in N–S direction differs significantly from their orientation in E–W direction (Fig. 4a–d). The remarkable N–S directed thrusts of reflection E4 (Fig. 7), which do not occur in E3 and which do not affect the uppermost evaporitic sequence, can be explained by a northbound displacement during the Messinian, caused, e.g., by gravity gliding that forced the young and 'wet' evaporites to creep downslope towards the basin centre. Such young and wet evaporites are supposed to have very low internal shear strength. On the other hand, numerical models of salt tectonics driven by sediment load show that post-depositional gravity gliding of salt occurs with vertically different gliding velocities depending on the assumed flow dynamics (Gemmer et al., 2004). Consequently, if Poiseuille or combined Poiseuille–Couette dominated salt flow is assumed, the highest gliding velocities occur in the middle of the salt body. If this model applies to the evaporites in the Levantine Basin, the northbound contraction of intra-salinar sequences observed in the centre of the basin can be also explained by Post-Messinian, i.e. post-depositional, deformation. However, since the thrusts did not penetrate or even affect the uppermost evaporitic sequence, we rule out this possibility.

In E–W direction the intra-salinar reflections run subparallel to the N-reflection. They dip basinward and

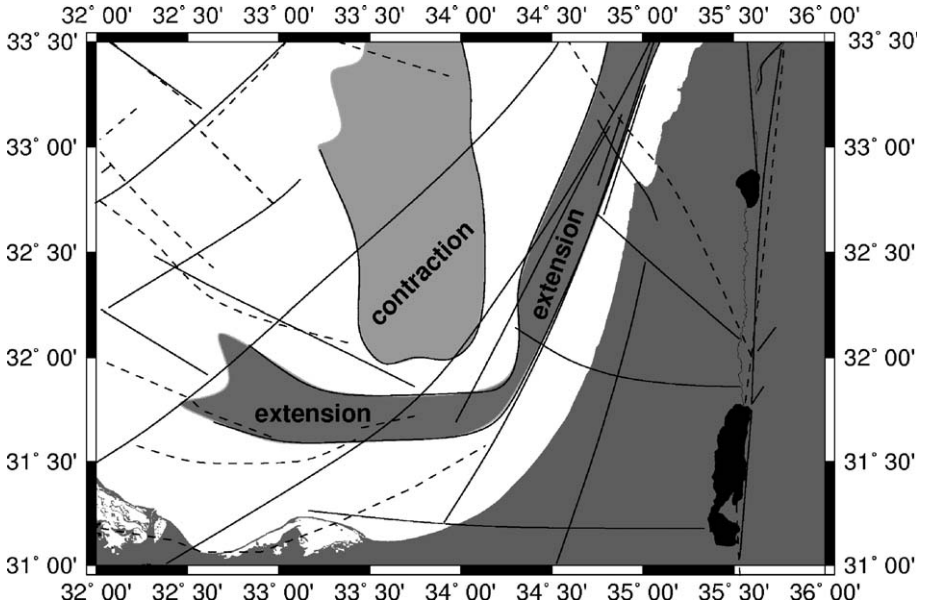

Fig. 12. Map of extensional and compressional features observed in the Pliocene–Quaternary, based on seismic lines of this study (Fig. 3a). No distinction between deep-rooted and salt-related structures has been made in this map. Between the 'belt of extension' and the zone of contraction, a corridor of comparatively low deformation is observed. Solid lines and dashed lines represent fault lines postulated by Neev (1975, 1977), Neev et al. (1976), and Abdel Aal et al. (2000), respectively. See Fig. 2 for labels. Note how the eastward boundary of the belt of extension corresponds to the course of Shelf Edge Hinge line, and the southern boundary to the Abdel Aal 5-fault.

toplap the M-reflection in the landward direction. The subsidence analysis indicates that in E–W direction little lateral displacement took place. Therefore, the geometry of the basinal evaporites can be restored by removing this sediment load (Fig. 6). Consequently, the E–W lines give the better picture of the status of the evaporites after the Messinian.

The backstripping analysis of the evaporites gives an idea how the individual evaporitic sequences were deposited. Assuming simple isostatic compensation of the evaporite load, i.e. without crustal flexure response or additional differential subsidence, the lower 4 sequences were deposited parallel to the slope with a westward dipping upper boundary (Fig. 9a–g). The question arises whether salt can be deposited with a non-horizontal surface or not. A horizontal deposition seems to be more likely since the salt precipitates from a brine with a high salt concentration. If we assume a westward tilt of the basin after a horizontal deposition of the lower 4 sequences, the uppermost sequence was also horizontally deposited, which also explains its westward increasing thickness (Fig. 9h–l). A westward tilt of the Levantine Basin in the Late Messinian would be isochronous to the major geodynamic changes in that realm like the transition from contraction to strike-slip tectonics along the eastern Cyprus Arc (Hall et al., 2005) or the onset of seafloor spreading in the Red Sea (Bosworth et al., 2005). Generally, a tilt of the basin could also be caused by subduction of thicker crust at the Cyprus Arc or by underthrusting.

On the eastern basin margin, the sequences reveal a basinwards prograding pattern. No basinal evaporites are present at a depth of less than 1800–1900 m after the backstripping of the Pliocene–Quaternary sediment prism. In general, several explanations are possible, e.g., basin subsidence or a sea level drop of almost this amount. However, this contradicts the results of two-dimensional stratigraphic simulations which led to the assumption of a sea level drop by 800–1300 m (Ben-Gai et al., 2005). Another explanation is erosion of the evaporites during the Post-Messinian transgression event or by currents parallel to the coast. Finally, a syn-depositional and basinward creep might also considered.

5.3. Post-Messinian deformation

For the discussion of the post-Messinian deformation we divide our study area into five regions: the eastern margin, the central basin, the Cyprus Arc and the Nile Scarp around the Eratosthenes Seamount. We further discuss the Israeli Slump Complex and the St. Pauli mud volcano.

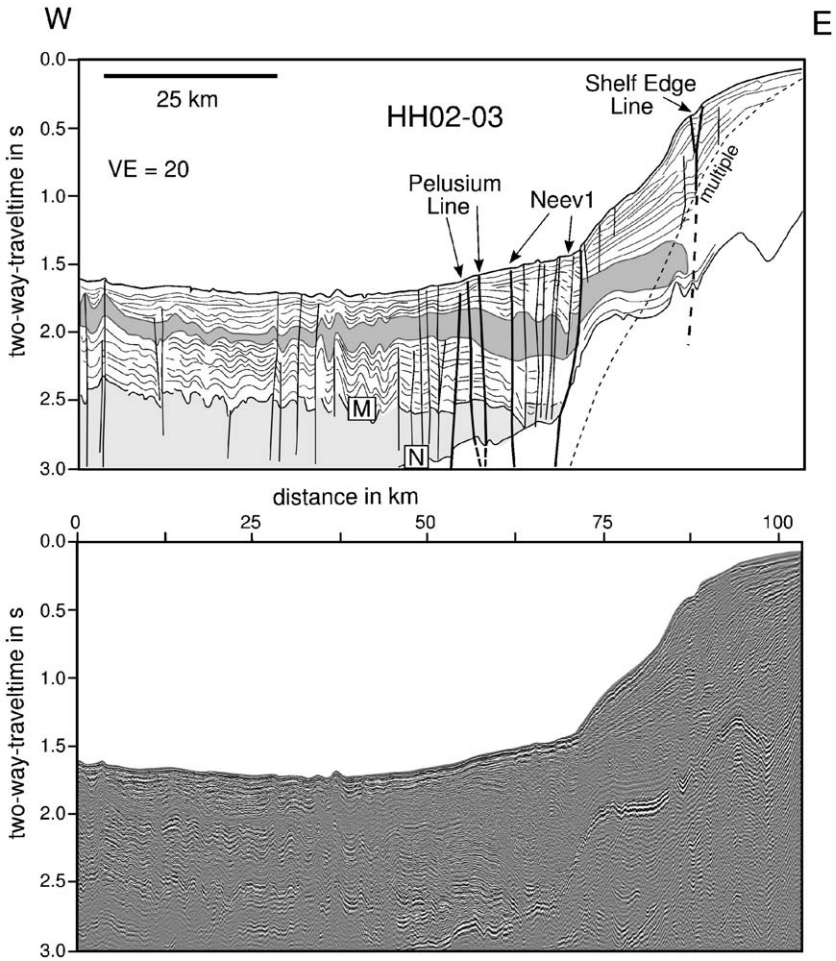

Fig. 13. Section of time migrated seismic line (below) and line drawing (above) of profile HH02-03. Top and bottom of the evaporite layer are indicated by M, and N, respectively, and the seafloor multiple is marked by the dashed line. Faults penetrating the evaporite layer coincide with the position of the Pelusium Line and the Neev 1 fault. The Shelf Edge Hinge Line is also well expressed. The area shaded in light grey corresponds to the evaporite body. The area shaded in darker grey indicates the slump body. A transition of the slump body into a transparent layer is observed, this layer can be traced well into the basin.

5.3.1. Eastern Margin

Extensional features such as normal and listric growth faults and keystone grabens are observed at the margin, forming a corridor of extension parallel to the coastline (Fig. 12). Both thin-skinned and thick-skinned tectonics have to be considered. As it is discussed by Gradmann et al. (2005) and as it is confirmed by the backstripping analysis in this study, some lateral displacements of the basinal evaporites occur southwest of Haifa along line HH02-01 (Fig. 6). The N-reflection represents the detachment fault. Salt rollers and salt welds evolved where the evaporites have been withdrawn. The presence of brittle upper evaporites and the observed turtle structures led to an adapted model of Letouzey et al. (1995) (Fig. 13 of Gradmann et al., 2005). Further south a lateral displacement did not occur and no salt welds evolved (e.g., Figs. 6 and 13). The extension of the upper basinal evaporites and the overburden probably represent an earlier stage of salt tectonics, because the thickness of the overburden is less than in the north. Compared to line HH02-01, the pinchout of the evaporites beneath the overburden occurs further downslope where the differential load is less significant. The evaporites are distorted but not withdrawn. This is in accordance to the numerical models of Gemmer et al. (2004), which show similar extensional features after 5 Ma in similar settings.

However, purely salt tectonic models do neither explain the faults that pierce the N-reflection nor the

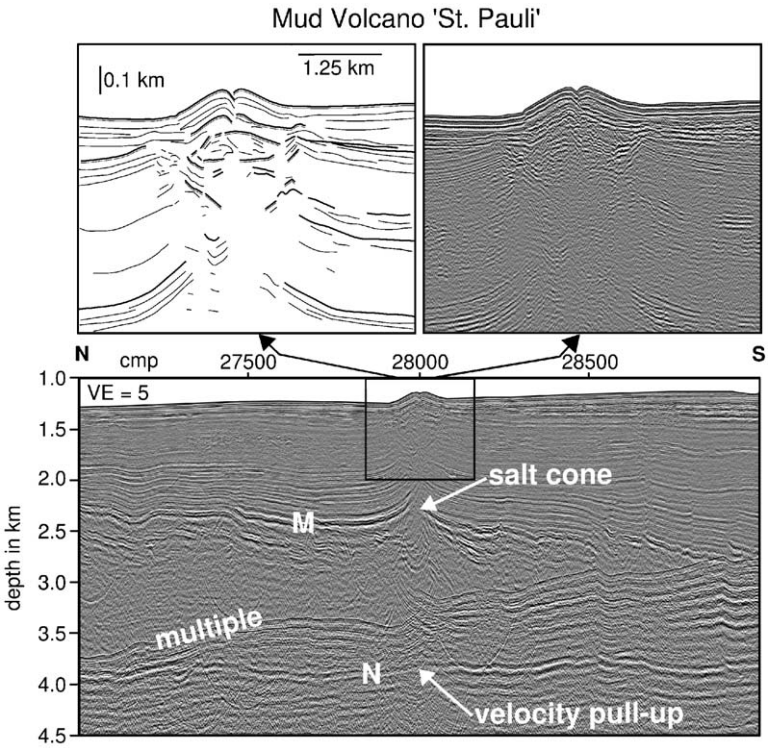

Fig. 14. Mud Volcano 'St. Pauli'. Upper left: line drawing of a close-up of the mud volcano. Upper right: seismic image, depth migrated, of the mud volcano. Both flanks are almost symmetric. Reflections underneath the mud volcano are bent upwards. Bottom: depth migrated seismic section of line HH04-06, showing the position and surroundings of the mud volcano and the salt cone. Top and bottom of the evaporite layer are indicated by M, and N, respectively.

growth faults that are above disturbed, but laterally continuous basinal evaporites as on line HH02-10 (Fig. 10). Since the M-reflection is at the same depth level on both sides of the faults, extension owing to differential subsidence can be ruled out. Faults that cut through the entire basinal evaporites without

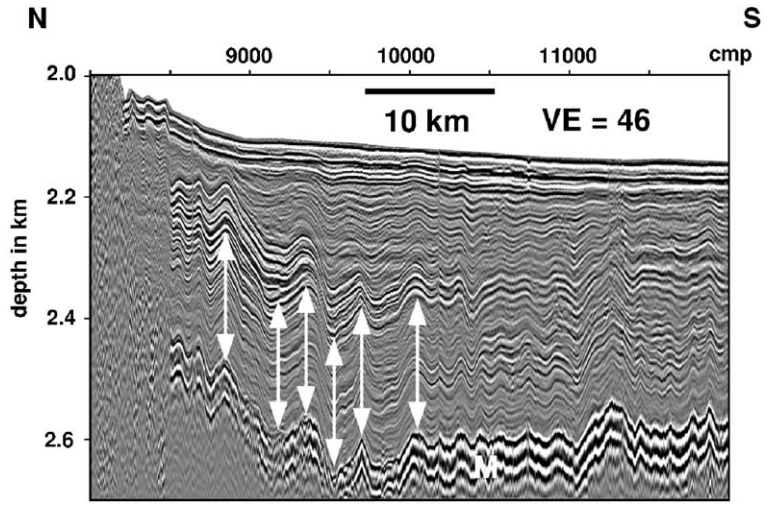

Fig. 15. A depth migrated section of seismic line HH04-06, showing a close-up of the Pliocene–Quaternary near the Cyprus Arc. The lower part of the Post-Messinian sediments of roughly 220 m shows the same deformation patterns as the M-reflection (indicated by the white M). The sediment package above shows a decrease in deformation up to about 50–100 m below the seafloor. The uppermost sediments appear almost flat.

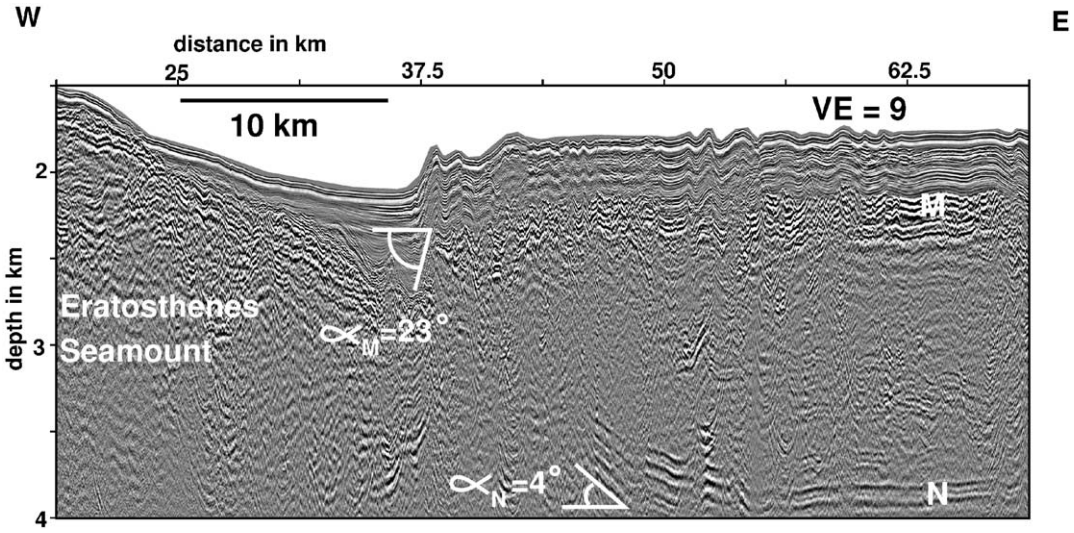

Fig. 16. Section of seismic line HH04-08, depth migrated, showing the Eratosthenes Seamount. Top and bottom of evaporite layer are indicated by M, and N, respectively. The M-reflection is severely distorted, whereas the N-reflection is comparatively smooth, rising at an angle of about 4°, which matches the slope of the seamount. Note the steep decline of M near the seamount, importing an angle of 23° (vertical exaggeration is 9) of the top of the evaporite body.

affecting the N-reflection can also not be explained by accompanied rollover folding or antithetic normal faults, since salt tectonic should cause mainly ductile deformation.

Active transform or transcurrent faults represent an explanation of thick-skinned tectonics as suggested by other authors (Neev, 1975; Neev et al., 1976; Neev, 1977; Abdel Aal et al., 2000) (Fig. 2). The strongest evidence of active thick-skinned tectonics is found in the southernmost survey area. South of 32° the Syrian Arc and Pelusium Line bends further to the west, which represent a right stepover. The dominant anticline and the horst (Fig. 11) can be considered as contractional ramps. As already proposed by Neev (1975), the transpression is a direct consequence of northward wedging of the crustal segments bounded to the east and west by the Dead Sea Transform Fault, the Pelusium Line and the Damietta–Latakia Line, respectively. Seafloor piercings of the main faults represent compelling evidence of neotectonic activity, which is not surprising because the DST is also an active fault. Contrary to the Pelusium and Neev1 Line, the Shelf Edge Hinge Line runs subparallel to the DST and it reveals extension. The growth fault in Fig. 10 is right above the Hinge Line and can be also explained by transtension or block rotating.

Consequently, we suggest that those folds and faults which affect the upper Pre-Messinian as well as the basinal evaporites and the Pliocene–Quaternary cover sequences are the consequence of active strike-slip tectonics. Northwest of Haifa, the strike-slip faults (Fig. 5) merge with the fault zone that reaches from the Carmel structure to south of Beirut (Schattner et al., submitted for publication) (Fig. 2).

5.3.2. Basinal contraction

There is an abundance of contractional folds, faults and thrusts in the basin (Figs. 7, 8, and 16). In E–W direction, Gradmann et al. (2005) also observed extensional structures near the shelf and pop-up structures and overthrusting in the basin, which complies with the models of Letouzey et al. (1995) of moving salt. However, the backstripping analysis suggests that little westward salt flux occurred in the Levantine Basin except directly southwest of Haifa. In N–S direction, however, on line HH04-06, the backstripping of the sediment load reveals that the evaporite body is first reduced by about 200 m near the pinchout and then thickened by about 200 m. The orientations of the thrusts within the evaporites are also different depending on the orientation of the seismic profile. While the thrusts are oriented basinwards on the S–N profiles, no specific orientation is observed on the E–W profiles. This suggests that the evaporites have been squeezed northwards by the sediment load and accumulated approx. 50 km to the north. The northbound creep of the evaporites can be explained by the particularly thick sediment load near the Nile Fan of almost 3 km compared to about 1 km on the shelf off Israel. The relation between the high sedimentation rate

in the Nile Fan and the initiation of gravity gliding has already been shown by Gaullier et al. (2000). The pop-up structures and overthrusting observed on the E–W profiles represent probably out-of-plane movement. At the Eratosthenes Seamount the basin is narrower than north or south of it, like a bottleneck for the S–N flow of the evaporites. However, since the orientation of the bathymetry and the evaporite thickness in the Levantine Basin is not exactly S–N, but SSW–NNE (Fig. 3a and c), it seems plausible that SSW–NNE is actually the main direction of salt movement (Fig. 17).

5.3.3. Israeli Slump Complex

Slump masses have been found on several lines, and slumps in the south of the Levantine Basin have been described by Frey-Martinez et al. (2005). On our lines, these slump masses can be correlated with a transparent layer that is present throughout the entire basin (Fig. 13). A significant number of faults which have been initiated isochronously to the slump bodies are found in the basin. These faults have been mapped on the entire data set and they are present up to 140 km away from the slump. We suggest that the onset of contraction associated with the ISC. Slumping causes the relocation of large amounts of sediments, which then leads to a sudden change in sediment load on the evaporites at the basin margin. It is well conceivable that in order to compensate the increased differential load after the slumping, abrupt movements in the evaporites are triggered. In this case, the initiation of salt movement in the Levantine Basin would be a consequence of the slumping.

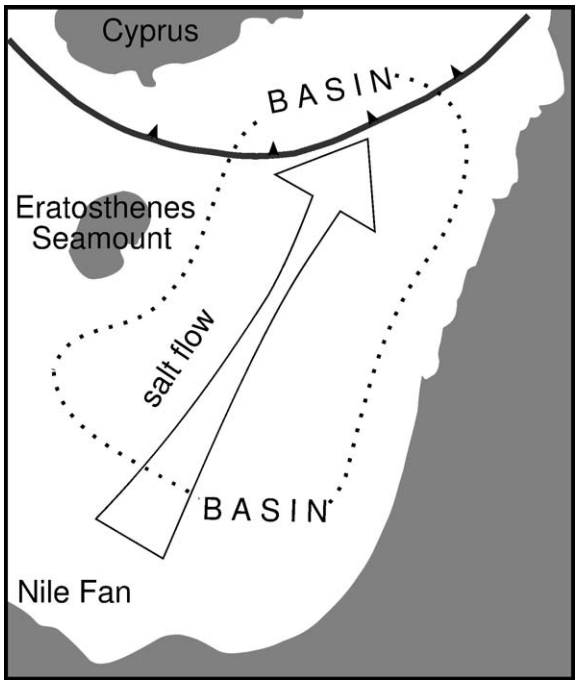

Fig. 17. Sketch visualising the postulated NNW–SSE salt flow in the Levantine Basin towards the Cyprus Arc. The thinning of the arrow represents the bottleneck effect of the Eratosthenes Seamount on the salt flow.

5.3.4. Cyprus Arc

The N-reflection is exceedingly deformed over a distance of 50 km and the M-reflection over a distance of 25 km. The seafloor, however, is flat. This indicates that compression abated since the Messinian and has now ceased completely. The sediments down to 50 to 100 mbsf are undisturbed, with the rough estimate of a constant sedimentation rate since the Messinian. This means that the contraction at the Cyprus Arc stopped at least 1 Ma ago. Two models may explain the contraction here: 1) thick-skinned (plate tectonic) basin shortening due to the subduction at the Cyprus Arc and 2) thin-skinned tectonics (salt tectonics) owing to the northward creep. According to the models of Gemmer et al. (2004), an increased deformation is expected far in the north after some 10 Ma only. Hall et al. (2005) date the transition from a compressional to a transpressional regime at the Cyprus Arc to early-middle Pliocene, which is much earlier than the observations on line HH04-06 indicate. Consequently, we assume that the increased but partly ceased deformation at the Cyprus Arc is a consequence of thick-skinned tectonics.

5.3.5. Eratosthenes Seamount

Near the Eratosthenes Seamount, the situation is entirely different. The N-reflection appears comparatively flat and smooth until it merges into the flank of the seamount, while the M-reflection and the seafloor are strongly distorted. Hence, the deformation observed there has probably been caused by thin-skinned tectonics. Since there is no significant E–W movement of the evaporites, the E–W contraction observed at the Eratosthenes has probably been caused by the northward creep through the bottleneck between seamount and the Levantine margin. It is a remarkable fact that no salt glaciers or salt tongues escaped from the evaporites into the Nile Scarp.

5.3.6. St. Pauli mud volcano

Mud volcanoes and cold seeps are common features in the Mediterranean Sea (see Limonov et al., 1996; Kopf et al., 1998; Coleman and Ballard, 2001; Loncke et al., 2004; Huguen et al., 2005). Loncke et al. (2004) found mud volcanoes on the Nile Deep Sea Fan in an

extensive regime where salt is absent or above growth faults. In an extensive regime, fluid paths from deeply buried reservoirs to the seafloor may exist where salt is absent as a result of gravity gliding or where active faults, e.g. growth faults, cut through the entire succession of subsalt, salt and overburden. At the St. Pauli mud volcano, the evaporites are not significantly thinned and still 1.5 km thick. There is no evidence of a growth fault in the seismic image and the base of the evaporites appears undisturbed. Therefore the fluid path of this mud volcano needs another explanation than those given by Loncke et al. (2004).

The presence of the seismically transparent cone on the upper evaporites and beneath the mud volcano suggests a correlation between these two features, which implies a fluid escape from or through the evaporites. In most settings salt represents an impermeable and sealing sequence. On the other hand, salt is permeable for fluids if the fluid pressure is above the lithostatic pressure, because the tensile strength of salt is negligible (J. Urai, pers. comm.). Fluid migration through a solid sequence of Messinian evaporites has already been proposed by Gradmann et al. (2005). This seismically transparent cone might be caused by diapirism, but because of its geometry the cone would rather represent a salt pillow than a diapir. However, the reflections below the cone are not bent upwards as would be typical for a diapiric feature. We suggest another explanation: The cone atop the M-reflection and beneath the mud volcano could consist of salt which has precipitated from fluids that escape from the evaporites and which feed the mud volcano. This interpretation and the observed sediment thickness of less than 1000 m above the salt cone suggest a fluid reservoir within or beneath the evaporites.

Murton and Biggs (2003) presented a simple numerical model for the formation of conical-shaped mud volcanoes. Based on the concept of isostatic equilibrium, this model allows an assessment of the depth of the mud source from the height of a mud volcano above the seafloor and the density of the underlying sediments (Eq. (2)).

$$h_{s2} = (h_v(\rho_{mud}-\rho_w)-h_{s1}(\rho_{s1}-\rho_{mud}))/(\rho_{s2}-\rho_{mud}) \quad (2)$$

Here, ρ_{mud} denotes the density of the mud, ρ_w the density of water, ρ_{s1} the density of the upper sediments, and ρ_{s2} the density of the lower sediment (in this case evaporites). The height of the mud volcano is h_v, the water depth is h_w, the thickness of the upper sediment layer is denoted by h_{s1}, and the thickness of the lower sediment layer from the top to the mud source is represented by h_{s2}.

We assumed densities of 1.8–2.0 kg/m^3 for the upper sediments, and 2.2 kg/m^3 as an average for the evaporites. These densities have been used for gravity modelling in the Levantine Basin (Ben-Avraham et al., 2002; Netzeband et al., 2006). The sediment density also corresponds with borehole measurements at the Napoli mud volcano on the Eastern Mediterranean Ridge (Kopf et al., 1998). The density of the mud must be greater than the density of the upper sediments but not the same as the density of the evaporites as required by the equation of Murton and Biggs (2003). A mud density 0.1–0.2 kg/m^3 greater than the sediment density, i.e. e. 1.9–2.1 kg/m^3 yields a depth of the mud source within the evaporite layer. If the mud source were deeper than the base of the evaporites, the sediment density would have to be lower, e.g. 1.7 kg/m^3, and the mud density at least 0.3 or the mud kg/m^3 greater than the sediment density.

Murton and Biggs (2003) considered their model applicable to all conical-shaped mud volcanoes, but it has to be emphasized that it is a very simple model, which gives only a rough idea of the depth of the mud source. Also, the seafloor shows only little downward flexure around the St. Pauli mud volcano, which might be an indication that isostatic compensation of the load of the erupted mud is not the only mechanism. E.g. it is conceivable that there had been an initial explosive eruption, which would have left a crater over which the mud volcano could have formed. This could explain the upward bending of the reflections beneath the mud volcano.

Although a mud source beneath the evaporite layer cannot be ruled out, the estimated depth of the mud source and the seismic image corroborate our interpretation of fluid sources beneath the top of the evaporites. An overpressurized fluid source within the evaporites can be explained by dewatering of young and wet salt, by gypsum-anhydrite conversion, or by the presence of intercalated water bearing sediments. Fluid pressure above the lithostatic pressure may also result from undercompacted and heated subsalt sediments. Overpressuring from plate-tectonics could result from transpressional strike-slip faulting along the Pelusium Line. For further investigation of the formation of St. Pauli, samples of the mud and of the surrounding sediments would be valuable.

6. Conclusions

The Messinian evaporitic succession reveals five evaporitic sequences, separated by four internal reflections traceable throughout the entire Levantine Basin.

The interpretation of the sequences as deposited during five depositional cycles is consistent with onshore drillings. The 4 internal reflections and M represent 4 facies changes caused by changes in brine salinity corresponding to temporal sea level rises. This led to an interbedding of the thick halite layers with rigid evaporites or clastic sediments or both. Each sequence was independently folded and faulted in a northern direction. We conclude that syn-depositional deformation occurred, e.g., lateral basinward creep caused by gravity forcing.

W–E striking seismic lines show basinward dipping internal reflections. However, the top of the evaporites, the M-reflection, runs horizontally and the uppermost sequence thickens to the west. This depositional pattern can be explained by horizontally deposited evaporitic sequences and a basinward tilt of the Levantine Basin during the Late Messinian, before the last and upper sequence precipitated. This tectonic event might be correlated with the overall changes of the geodynamic setting in the Middle East during that time.

Off Israel and from south to north the sediment load on the edge of the basinal evaporites increases, since the marginal pinchout has been shifted from beneath the lower slope to beneath the shelf. The apparent rollback folding, however, is a consequence mainly of differential subsidence and not of lateral displacement of the evaporites and thin-skinned extension, respectively.

The northward increasing differential sediment load allows the study of initial salt tectonics in succeeding evolutionary stages. Off southern Israel, only the Pliocene–Quaternary sediment cover shows extensional faults and the upper evaporites are little deformed. In general, very little basinward displacement occurred to the west. Off northern Israel and right south of Haifa the presence of salt welds and salt rollers gives evidence of the displacement of the entire basinal evaporites.

After backstripping the Pliocene–Quaternary and the evaporite layer, the Pre-Messinian seafloor is 1800–1900 m deep. This suggests that the sea level drop during the Messinian Salinity Crisis might have been greater than the previously assumed maximum of 1300 m. Alternatively, the evaporites could have been eroded or displaced during or directly after deposition, before they were covered by Pliocene sediments.

The load of the Nile Fan sediments squeezes the evaporites into an NNE direction parallel to the bathymetric gradient of the basin. In front of the lower fan, the evaporites are thickened due to forebulging. However, even here the rollback folding is mainly a seeming feature. The decline of the top of the evaporites beneath the Nile Fan is caused by differential subsidence.

The remobilization and depositing of the sediments from the Israeli Slump Complex on the edge of the evaporites coincides with the onset of contractional faulting of upper evaporites and overburden up to 140 km away from the slumps. We therefore suggest a causative correlation.

A seismically transparent cone on the top of the evaporites and beneath the St. Pauli mud volcano is interpreted as salt which has precipitated from fluids escaping from the evaporites. Since the thickness of the evaporites is about 1500 m, the fluid reservoir must lie within the evaporites, or the fluids migrate through the entire evaporitic succession.

Several strike-slip faults like the Pelusium, Shelf Edge Hinge and Neev1 Lines, which run subparallel to the Israeli slope are tectonically active. The faults overprint the entire succession of evaporites and overburden. Where the Pelusium Line bends further to the West, transpression occurs resulting in uplifted horsts and anticlinal folding.

Acknowledgements

We would like to thank the masters, crews and scientific staff of *RV Meteor* and *RV Pelagia* for the excellent support during the surveys. Thanks to Zvi Ben-Avraham, Zvi Garfunkel and Janos Urai for the initial ideas. Special thanks to Lea Scharff for carrying out the depth migration. We want to thank Jeremy Hall and an anonymous reviewer for valuable comments, which greatly improved the manuscript. Figs. 1–3, and 6 were created with GMT (Wessel and Smith, 1998). The GEMME project was funded by DFG grant HU698/07. The SAGA cruise was funded by the University of Hamburg.

References

Abdel Aal, A., El Barkooky, A., Gerrits, M., Meyer, H., Schwander, M., Zaki, H., 2000. Tectonic evolution of the eastern Mediterranean Basin and its significance for hydrocarbon prospectivity in the ultradeepwater of the Nile Delta. Lead. Edge 19, 1086–1102.

Allen, P.A., Allen, J.R., 1990. Basin Analysis — Principles & Applications. Blackwell Scientific Publications, Oxford. 463 pp.

Almagor, G., 1984. Salt controlled slumping on the Mediterranean slope of central Israel. Mar. Geophys.Res. 6, 227–243.

Almagor, G., 1993. Continental slope processes off northern Israel and southernmost Lebanon and their relation to onshore tectonics. Mar. Geol. 112, 151–169.

Ben-Avraham, Z., Tibor, G., Limonov, A.F., Leybov, M.B., Ivanov, M. K., Tokarev, M.Yu, Woodside, J.M., 1995. Structure and tectonics of the eastern Cyprean Arck. Mar. Pet. Geol. 12, 263–271.

Ben-Avraham, Z., Ginzburg, A., Makris, J., Eppelbaum, L., 2002. Crustal structure of the Levant Basin, eastern Mediterranean. Tectonophysics 346, 23–43.

Ben-Gai, Y., Ben-Avraham, Z., Buchbinder, B., Kendall, C.G.St.C., 2005. Post-Messinian paleodepth reconstruction of the Levantine margin off Israel. Mar. Geol. 221, 359–379.

Bosworth, W., Huchon, P., McClay, K., 2005. The Red Sea and Gulf of Aden Basins. J. Afr. Earth Sci. 43, 334–378.

Bridge, C., Calon, T.J., Hall, J., Aksu, A.E., 2005. Salt tectonics in two convergent-margin basins of the Cyprus Arc. Northeastern Mediterranean. Mar. Geol. 221, 223–259.

Clauzon, G., Suc, J.-P., Gautier, F., Berger, A., Loutre, M.-F., 1996. Alternate interpretation of the Messinian salinity crisis; controversy resolved. Geology 24, 363–366.

Cohen, A., 1993. Halite–clay interplay in the Israeli Messinian. Sediment. Geol. 86, 211–228.

Coleman, D.F., Ballard, R.D., 2001. A highly concentrated region of cold hydrocarbon seeps in the southeastern Mediterranean Sea. Geo Mar. Lett. 21, 162–167.

Dercourt, J., Zonenshain, L.P., Ricou, L.E., Kazmin, V.G., Le Pichon, X., Knipper, A.L., Grandjacquet, C., Sbortshikov, I.M., Geyssant, J., Lepverier, C., Pechersky, D.V., Boulin, J., Sibuet, J.C., Savostin, L.P., Sorokhtin, D., Westphal, M., Bazhenov, M.L., Laurer, J.P., Bijou-Duval, B., 1986. Geological evolution of the Tethys belt from the Atlantic to the Pamirs since the Lias. Tectonophysics 123, 241–315.

Dimitrov, L., Woodside, J., 2003. Deep sea pockmark environments in the eastern Mediterranean. Mar. Geol. 195, 263–276.

dos Reis, A., Gorini, T., Mauffret, C., 2005. Implications od salt–sediment interactions on the architecture of the Gulf of Lions deep-water sedimentary systems— western Mediterranean Sea. Mar. Pet. Geol. 22, 713–746.

Druckman, Y., Buchbinder, B., Martinotti, G.M., Siman Tov, R., Aharon, P., 1995. The buried Afiq Canyon (eastern Mediterranean, Israel): a case study of a Tertiary submarine canyon exposed in Late Messinian times. Mar. Geol. 123, 167–185.

Frey-Martinez, J., Cartwright, J., Hall, B., 2005. 3D seismic interpretation of slump complexes: examples from the continental margin of Israel. Basin Res. 17, 83–108.

Gardosh, M., Druckmann, Y., in press. Stratigraphy and tectonic evolution of the Levantine Basin, offshore Israel. In: A. Robertson (Ed), Tectonic Development of the Eastern Mediterranean Region, Geological Society Special Publication.

Garfunkel, Z., 1984. Large-scale submarine rotational slumps and growth faults in the Eastern Mediterranean. Mar. Geol. 55, 305–324.

Garfunkel, Z., 1998. Constraints on the origin and history of the Eastern Mediterranean basin. Tectonophysics 298, 5–35.

Garfunkel, Z., 2004. Origin of the Eastern Mediterranean basin: a reevaluation. Tectonophysics 391, 11–34.

Garfunkel, Z., Almagor, G., 1984. Geology and Structure of the continental margin off northern Israel and the adjacent part of the Levantine Basin. Mar. Geol. 62, 105–131.

Garfunkel, Z., Arad, A., Almagor, G., 1979. The Palmahim Disturbance and its regional setting. Bull. - Geol. Surv. Isr. 72, 56.

Gaullier, V., Mart, Y., Bellaiche, G., Mascle, J., Vendeville, B.-C., Zitter, T., Benkhelil, J., Buffet, G., Droz, L., Ergun, M., Huguen, C., Kopf, A., Levy, R., Limonov, A., Shaked, Y., Volkonskaia, A., Woodside, J., 2000. In: Vendeville, B.-C., Mart, Y., Vigneresse, J.-L. (Eds.), Salt, Shale and Igneous Diapers in and Around Europe: Geological Society of London, Geological Society Special Publication, vol. 174, pp. 111–129.

Gemmer, L., Ings, S.J., Medvedev, S., Beaumont, C., 2004. Salt tectonics driven by differential sediment loading: stability analysis and finite element experiments. Basin Res. 16, 199–218.

Gradmann, S., Hübscher, C., Ben-Avraham, Z., Gajewski, D., Netzeband, G.L., 2005. Salt tectonics off northern Israel. Mar. Pet. Geol. 22, 597–611.

Gvirtzman, G., Buchbinder, B., 1978. The Late Tertiary of the coastal plain and continental shelf of Israel and its bearing on the history of the Eastern Mediterranean. In: Ross, D.A., Neprochov, Y.P. (Eds.), Init. Repts. DSDP, vol. 42 II. U.S Govt. Printing Office, Washington D.C., pp. 1195–2220.

Hall, J., Calon, T.J., Aksu, A.E., Meade, S.R., 2005. Structural evolution of the Latakia Ridge and Cyprus Basin at front of the Cyprus Arc, Eastern Mediterranean Sea. Mar. Geol. 221, 261–297.

Hirsch, F., Flexer, A., Rosenfeld, A., Yellin-Dror, A., 1995. Palinspastic and crustal setting of the eastern Mediterranean. J. Pet. Geol. 18, 149–170.

Hsü, K.J., Cita, M.B., Ryan, W.B.F., 1973. The origin of the Mediterranean evaporites. In: Ryan, W.B.F., Hsü, K.J. (Eds.), Init. Repts. DSDP, vol. 13. U.S. Govt. Printing Office, Washington D.C., pp. 1203–1232.

Hsü, K.J., Monadert, L., Bernoulli, D., Cita, B.C., Erickson, A., Garrison, R.E., et al., 1978. History of the Mediterranean Salinity Crisis. In: Hsü, K.J., Montadert, L. (Eds.), Init. Repts. DSDP, vol. 42 I. U.S. Govt. Printing Office, Washington D.C., pp. 1053–1078.

Huguen, C., Mascle, J., Woodside, J., Zitter, T., Foucher, J.-P., 2005. Mud volcanoes and mud domes of the Central Mediterranean Ridge: near-bottom and in situ observations. Deep-Sea Res. I 52, 1911–1931.

Jiménez-Munt, I., Sabadini, R., Gardi, A., Bianco, G., 2003. Active deformation in the Mediterranean from Gibraltar to Anatolia inferred from numerical modeling and geodetic and seismological data. J. Geophys. Res. 108, 2006. doi:10.1029/2001JB001544.

Kempler, D., Garfunkel, Z., 1994. Structures and kinematics in the northeastern Mediterranean: a study of an unusual plate boundary. Tectonophysics 234, 19–32.

Kopf, A., Clennell, M.B., Camerlenghi, A., 1998. Variations in sediment physical properties and permeability of mud-volcano deposits from Napoli dome and adjacent mud volcanoes. In: Robertson, A.H.F., Emeis, K.-C., Richter, C., Camerlenghi, A. (Eds.), Proc. ODP, Sci Results, vol. 160. Ocean Drilling Program, College Station, TX.

Letouzey, J.B., Coletta, R., Chermette, J.C., 1995. Evolution of salt-related structures in compressional settings. In: Jackson, M.P.A., Roberts, D.J., Snelson, S. (Eds.), Salt Tectonics: A Global Perspective, vol. 65. AAPG Memoir Tulsa, Oklahoma, USA, pp. 41–60.

Limonov, A.F., Woodside, J.M., Cita, M.B., Ivanov, M.K., 1996. The Mediterranean Ridge and related mud diapirism: a background. Mar. Geol. 132, 7–19.

Loncke, L., Mascle, J., FANIL Scientific Party, 2004. Mud volcanoes, gas chimneys, pockmarks and mounds in the Nile deep-sea fan (Eastern Mediterranean): geological evidences. Mar. Pet. Geol. 21, 669–689.

Makris, J., Ben-Avraham, Z., Behle, A., Ginzburg, A., Giese, P., Steinmetz, L., et al., 1983. Seismic reflection profiles between Cyprus and Israel and their interpretation. Geophys. J. R. Astron. Soc 75, 575–591.

Mart, Y., 1984. The tectonic regime of the southeastern Mediterranean continental margin. Mar. Geol. 55, 365–386.

Mart, Y., 1987. Superpositional tectonic patterns along the continental margin of the southeastern Mediterranean: a review. Tectonophysics 140, 213–232.

Mart, Y., Ben-Gai, Y., 1982. Some depositional patterns at the continental margin of the Southeastern Mediterranean Sea. AAPG Bull. 66, 460–470.

Mascle, J., Benkhelil, J., Bellaiche, G., Zitter, T., Woodside, J., Loncke, L., 2000. Marine geologic evidence for a Levantine–Sinai plate, a new piece of the Mediterranean puzzle. Geology 28, 779–782.

Montadert, L., Letouzy, J., Mauffret, A., 1978. Messinian event: seismic evidence. Init. Repts. DSDP, vol. 42 I. U.S. Govt. Printing Office, Washington D.C., pp. 1032–1050.

Murton, B.J., Biggs, J., 2003. Numerical modelling of mud volcanoes and their flows using constraints from the Gulf of Cadiz. Mar. Geol. 195, 223–236.

Neev, D., 1975. Tectonic evolution of the Middle East and the Levantine basin (easternmost Mediterranean). Geology 3, 683–686.

Neev, D., 1977. The Pelusium Line — a major transcontinental shear. Tectonophysics 38, T1–T8.

Neev, D., Almagor, G., Arad, A., Ginzburg, A., Hall, J.K., 1976. The geology of the Southeastern Mediterranean Sea. Bull. - Geol. Surv. Isr. 68, 1–51.

Netzeband, G.L., Gohld, K., Hübscher, C.P., Ben-Avraham, Z., Dehghani, G.A., Gajewski, D., Liersch, P., 2006. The Levantine Basin— crustal structure and origin. Tectonophysics 418, 167–188.

Papazachos, B.C., Papaioannou, Ch.A., 1999. Lithospheric boundaries and plate motions in the Cyprus area. Tectonophysics 308, 193–204.

Pätzold, J., Bohrmann, G., Hübscher, C., 2003. Black Sea–Mediterranean– Red Sea. METEOR-Berichte 03-2, Leitstelle METEOR.

Polonia, A., Camerlenghi, A., Davey, F., Storti, F., 2002. Accretion, structural style and syn-contractional sedimentation in the Eastern Mediterranean Sea. Mar. Geol. 186, 127–144.

Réhault, J.P., Boillot, G., Mauffret, A., 1984. The western Mediterranean Basin, geological evolution. Mar. Geol. 55, 447–477.

Robertson, A.H.F., 1998. Tectonic significance of the Eratosthenes Seamount: a continental fragment in the process of collision with a subduction zone in the eastern Mediterranean (Ocean Drilling Program Leg 160). Tectonophysics 29, 863–882.

Robertson, A.H.F., Dixon, J.E., 1984. Introduction: aspects of the geological evolution of the Eastern Mediterranean. In: Dixon, J.E., Robertson, A.H.F. (Eds.), Geological Evolution of the Eastern Mediterranean: Geol. Soc. Spec. Publ. London, vol. 17, pp. 1–74.

Rouchy, J.-M., Saint Martin, J.-P., 1992. Late Miocene events in the Mediterranean as recorded by carbonate–evaporite relations. Geology 20, 629–632.

Ryan, B.W.F., Stanley, D.J., Hersey, J.B., Fahlquist, D.A., Allan, T.D., 1970. The tectonics of the Mediterranean Sea. In: Maxwell, A.E. (Ed.), The Sea, vol. 4 II. Wiley, New York, pp. 387–491.

Schattner U., Ben-Avraham Z., Lazar M., Hübscher, C., submitted for publication. Tectonic isolation of the Levant basin offshore Galilee-Lebanon— Effects of the Dead Sea fault plate boundary on the Levant continental margin, eastern Mediterranean.

Tibor, G., Ben-Avraham, Z., 2005. Late Tertiary paleodepth reconstruction of the Levantine margin off Israel. Mar. Geol. 221, 261–297.

Tibor, G., Ben-Avraham, Z., Steckler, M., Fligelmann, H., 1992. Late tertiary subsidence history of the southern Levant Margin, Eastern Mediterranean Sea, and its implications to the understanding of the Messinian Event. J. Geophys. Res. 97, 17593–17614.

Vidal, N., Alvarez-Marrón, J., Klaeschen, D., 2000a. Internal configuration of the Levantine Basin from seismic reflection data (Eastern Mediterranean). Earth Planet. Sci. Lett. 180, 77–89.

Vidal, N., Klaeschen, D., Kopf, A., Docherty, C., Von Huene, R., Krasheninnikov, V.A., 2000b. Seismic images at the convergence zone from south of Cyprus to the Syrian coast, eastern Mediterranean. Tectonophysics 329, 157–170.

Waltham, D., 1997. Why does salt start to move? Tectonophysics 282, 117–128.

Wessel, P., Smith, W., 1998. New, improved version of Generic Mapping Tools released, EOS. Trans. Am. Geophys. Union 79 (47), 579.

Woodside, J.M., 1977. Tectonics elements and crust of the Eastern Mediterranean Seamount. Mar. Geophys. Res. 3, 317–354.

Woodside, J.M., Mascle, J., Zitter, T.A.C., Limonov, A.F., Ergun, M., Volkonskaia, A., Shipboard scientists of the PRISMED II expedition, 2002. The Florence Rise, the western bend of the Cyprus Arc. Mar. Geol. 185, 177–194.